2013•2014
FACULTEIT INDUSTRIËLE INGENIEURSWETENSCHAPPEN
master in de industriële wetenschappen: elektromechanica

Masterproef

Electroactive properties of elastomers: finite element method modelling and experimental measurements

Promotor :
ing. Eric CLAESEN

Promotor :
Mr. PEDRO LLOVERA

Raphaël Vorias , Dimitri Letihon

Proefschrift ingediend tot het behalen van de graad van master in de industriële wetenschappen: elektromechanica

Gezamenlijke opleiding Universiteit Hasselt en KU Leuven

2013•2014
Faculteit Industriële ingenieurswetenschappen
master in de industriële wetenschappen: elektromechanica

Masterproef

Electroactive properties of elastomers: finite element method modelling and experimental measurements

Promotor :
ing. Eric CLAESEN

Promotor :
Mr. PEDRO LLOVERA

Raphaël Vorias , Dimitri Letihon
Proefschrift ingediend tot het behalen van de graad van master in de industriële wetenschappen: elektromechanica

universiteit hasselt | KU LEUVEN

Abstract

This study investigated different techniques to measure the displacement of a dielectric elastomer actuator (DEA) of the acrylic 3M tape VHB 4910 and compare these to a finite element model.

Elastomers have a non-linear stretch-strain relationship, which make them difficult to predict. Therefore, a credible computer model is needed to simulate the effects of actuation. Various methods exist to approximate the stress-strain behavior of elastomers. In this thesis the Ogden model based on free strain energy density will be used. The FE-model is made in Comsol Multiphysics.

Furthermore, working with very thin films calls for the need of an accurate test setup. Various improvements were made for the test setups and sample preparations. The displacements were measured with three methods: first with a vibrometer. Second, with an low frequency AC voltage superimposed on a DC voltage. And thirdly, with a digital camera.

Up until 2,5 kV, the Ogden model fits the vibrometer experimental data, but deviates after it reaches this point. This might be explained by the variable concentrations of carbon black, which cause defects in the electrostatic field. Furthermore, in order to have a better fit, the Ogden parameters could be optimized. Secondly, due to the very low intrinsic capacity of the DEA, the AC/DC superimposition proved to be unsuccessful.

Contents

List of Figures

List of Tables

1. Introduction

Dielectric elastomer actuators are electromechanical transducers able to convert electrical energy into mechanical energy and vice versa. The basic structure of a DEA is shown in Fig. 1.1. DEAs are basically a thin piece of insulating elastomer sandwiched between two compliant electrodes. In this thesis the acrylic polymer VHB 4910 will be the dielectric elastomer and carbon black will be used as electrode material.

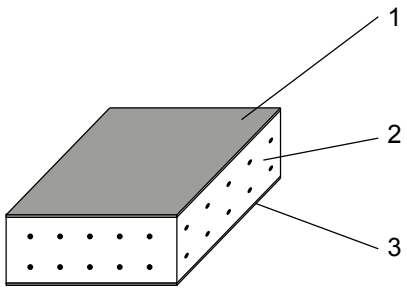

Figure 1.1.: Main components of a DEA: 1) Top electrode. 2) Dielectric elastomer. 3) Bottom electrode.

When a potential is put on the electrodes, the elastomer is subjected to an electrostatic pressure. This results in the DEA's thickness to decrease and its area to increase. The increase of area is due to the elastomer's incompressibilty. In other words, its volume does not change. From a pure electrical point of view, a DEA can be seen as a variable capacitor of which the dielectric material is an elastomer.

This thesis will be aimed at comparing actuation data of a dielectric elastomer actuator (DEA) from three experiments with a finite element model. In the first experiment, a laser vibrometer is used to measure the actuation from one side. In the second experiment, the actuated area is captured with a digital camera. Finally, AC-DC superimposition is used. chapter 2 explains each experiment setup and how the DEA was made. The finite element model is made in Comsol and is explained in detail in chapter 3.

1.1. Theoretical background

This section elaborates on some of the theoretical aspects of dielectric elastomer actuators and other concepts used in this thesis. First of all, Fig. 1.2 shows the coordinate system and how the lengths of the elastomer are defined. The coordinate system is Cartesian with axes named 1, 2 and 3. The initial dimensions are defined as L_1, L_2 and L_3.

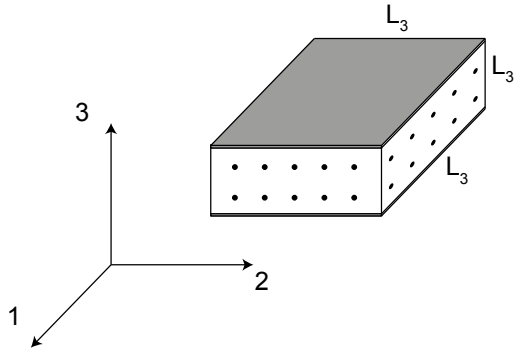

Figure 1.2.: DEA coordinate system.

Now consider the electrodes become charged with a voltage V . The top electrode then contains positive charges and the bottom electrode negative charges. Fig. 1.3 shows the initial state and the actuated state.

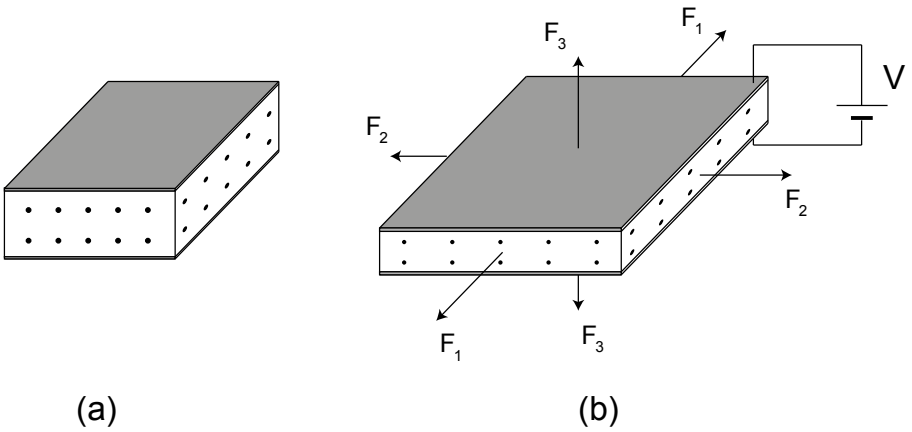

Figure 1.3.: The elastomer in initial state (a) and actuated state (b).

If L_1, L_2 and L_3 are the initial dimensions and suppose l_1, l_2 and l_3 the lengths in actuated state, then the strain is defined as:

$$\lambda_i = \frac{l_i}{L_i} \tag{1.1}$$

With $i = \{1, 2, 3\}$. Next, two assumptions are made. Firstly, the elastomer is assumed to be incompressible. In other words, the volume stays constant. This gives the relation:

$$\lambda_1\lambda_2\lambda_3 = 1 \tag{1.2}$$

So if the thickness reduces or $\lambda_3 < 1$, then the area must become larger or $\lambda_1\lambda_2 > 1$. Secondly, the elastomer is assumed to be isotropic. This means that the area becomes larger in both the first direction and the second direction. The equation is:

$$\lambda_1 = \lambda_2 \tag{1.3}$$

for stretches up to 7 [1]. These two assumptions explain why the elastomer grows uniformely larger in area when it reduces in thickness or vice versa. It is through this actuation, electrical energy is converted to mechanical energy. Physically interpreted, it comes from two effects. The first one is based on different charges attracting. This happens when the thickness reduces and the two plates come closer. The second one is based on like charges repelling. This manifests when the electrodes spread out [4].

1.1.1. Parallel plate capacitor

A capacitor is a device capable of storing electrical energy. The amount of energy that can be stored in a capacitor is called the capacitance and is expressed in Farads. A capacitor has a capacity of one Farrad when the charge in between its two plates is one Coulomb[1] and the voltage applied to the parallel plates is one Volt. The capacitance of the parallel plate capacitor can be determined by:

$$C = \frac{Q}{V} \tag{1.4}$$

When a voltage V is applied to the parallel plates, one plate will get a positive charge while the other one will get a negative charge, as can be seen in Fig. 1.4. When the space in between the parallel plates is vacuum, there is no material that can be polarized and the capacity can be determined by

$$C_0 = \varepsilon_0\frac{E}{V} \tag{1.5}$$

Now consider a capacitor with a certain material in between its parallel plates, as shown in Fig. 1.5.

[1]Coulomb: a unit to express electrical charge and is expressed in amperes per second. It is the amount of charge carried by an electrical current of one ampere during one second.

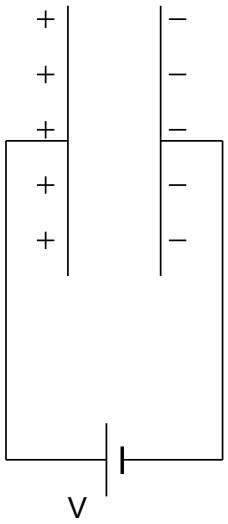

Figure 1.4.: Charges on a parallel plate capacitor with vacuum between the plates.

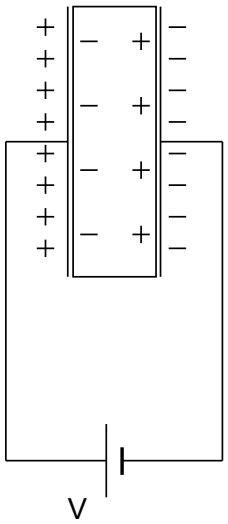

Figure 1.5.: Charges on a parallel plate capacitor with dielectric between the plates.

When a voltage is applied the material will reorganize its charges (electrons and protons) to a certain extent. Positive charges will be attracted towards the negative electrode and negative charges toward the positive electrode. This phenomenon is called polarization (or appearance of bond charges) of the material and it means that more energy can be stored on the electrodes of the capacitor for the same applied voltage. As a result, the capacitance of the system is increased by a factor ε_r, called the relative permittivity. The relative permittivity of a material is the ratio of the increased capacitance according to the vacuum capacitance. [5] The equation is:

$$\varepsilon_r = \frac{C}{C_0} \tag{1.6}$$

As DEAs can be considered as a thin film capacitance another approximation is made (this approximation is made for all thin film capacitances):

$$C = \varepsilon_r \varepsilon_0 \frac{A}{d} \tag{1.7}$$

This equation applies to a film for which the characteristics area to the thickness ratio satisfies [6]:

$$\frac{\sqrt{A}}{d} \ggg 1 \tag{1.8}$$

1.1.2. Transduction

As noted above, DEAs are able to transduce mechanical energy and in order for that to be accomplished, the electrodes must typically stretch and contract with the polymer. Thus, the electrodes have to be compliant. The ideal structure of a DEA can be assumed as two electrodes without any resistance and have perfect compliant properties. Furthermore, the elastomer should have high dielectric properties and on top of that have no mechanical losses. By means of this, there are no losses of energy but it is converted from one system to another during the changes of state. [7]

1.1.3. Failure modes

A DEA has certain operation limits. These are characterised by electrial breakdown, mechanical breakdown and pull-in failure.

1.1.3.1. Electric breakdown

Electrical breakdown is a phenomenon which occurs when the elastomer film loses its insulating properties and becomes a conductor. It is dominant in very low stretch rates that are not used in practice. Predictions by representing complex molecular and atomic interactions of the breakdown voltage are far too complex. This is why those values are mostly obtained experimentally. The dielectric failure is determined by breakdown voltage vs. stretch ratio of the elastomer. It should be noted that these tests are done with non-deforming electrodes. [1]

1.1.3.2. Mechanical breakdown

Mechanical breakdown is the tearing of the film when folded polymer chains are straightened beyond their unfolded length. Just like dielectric strength, the mechanical breakdown of the film has to be determined experimentally. Mechanical film deformation is limited by an experimentally determined maximum area expansion. For the VHB 4910 the following failure criteria can be considered:

$$\lambda^2 > 36 \tag{1.9}$$

In summary, this means that when the elastomer is stretched more than 600 %, mechanical failure will occur. [1]

1.1.3.3. Pull-in failure

Pull-in failure occurs when the electrostatic pressure becomes greater than the compressive strength of the elastomer. Before pull-in failure breaks the film, another phenomenon appears which is called pull-in instability. This instability mode is recognized as a complex 3D wrinkling pattern at the surface of the actuated area of the DEA, as can be seen in Fig. 1.6. Failure occurs when the film thickness falls below a certain threshold and the electrostatic pressure becomes very large, see Eq 1.17. The excessive deformations caused by pull-in will eventually lead to material or dielectric strength failure. [1]

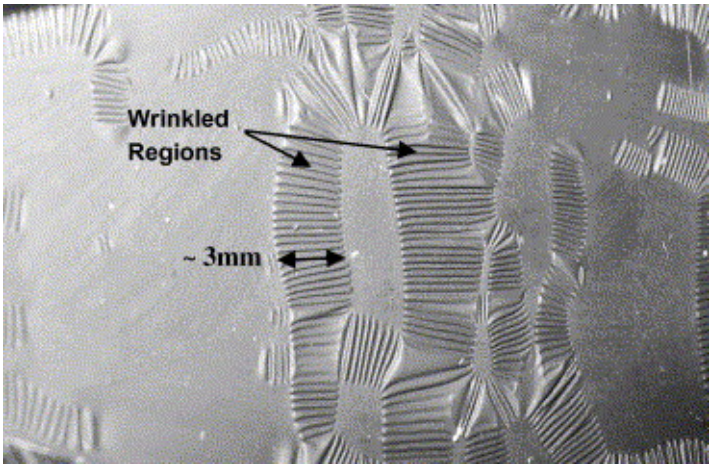

Figure 1.6.: The phenomenon of pull-in instabillity is clearly visible as vertical and horizontal wrinkles.[1]

Furthermore, pull-in is the dominant failure mode in low stretch ratios (up to 300 % pre-stretch), see Fig. 1.7. Last of all, it is also assumed that when pull-in instability starts, and the voltage is not removed, pull-in will eventually lead to failure after a certain amount of time. [1]

1.1.4. Pre-stretch

Pre-stretch means that the elastomer film is stretched during the manufacturing of the DEA sample. This means that the elastomer in between the electrodes is under constant tension. When the DEA is operating the area in between the electrodes will undergo an additional displacement. The plain area of the DEA will react on the behaviour of the operating area in between the electrodes, depending on the configuration of the DEA.

It is important that during actuation a certain amount of pre-stretch remains, because by pre-stretching the formation of wrinkles is prevented (not to confuse with the wrinkles that appear when the thickness of the membrane is reduced to zero)

by keeping the boundaries of the DEA membrane under tension during a change of state. Also, by pre-stretching the distance in between the electrodes is reduced, which provides a higher Maxwell tension under the same applied voltage. As a higher Maxwell tension results in a higher electric pressure, the deformation will remarkably improve. Finally, pre-stretching causes a shift in the curve of mechanical breakdown in the direction of the curve of electrical breakdown. In other words, it will be possible to detect mechanical breakdown. [8]

Fig. 1.7 shows that when the pre-stretch ratio reaches $\lambda^2_{pre} = 9$, the pull-in phenomenon is eliminated, allowing very large area expansions. Fig. 1.7 shows that the biggest actuation area expansion is when $\lambda^2_{pre} = 10$, and allowing area expansions up to $\lambda^2_{pre} = 4,29$.

It has been shown experimentally that pre-stretch has the effect of increasing the electric breakdown field up to one order of magnitude. [9, 2]Therefore, a higher voltage can be applied to the electrodes, which results in a higher electrostatic pressure. Thus, by increasing the dielectric breakdown we automatically improve the actuation properties of the DEA. Simply put, when the dielectric properties are increased a higher voltage can be applied, increasing the electrostatic pressure.

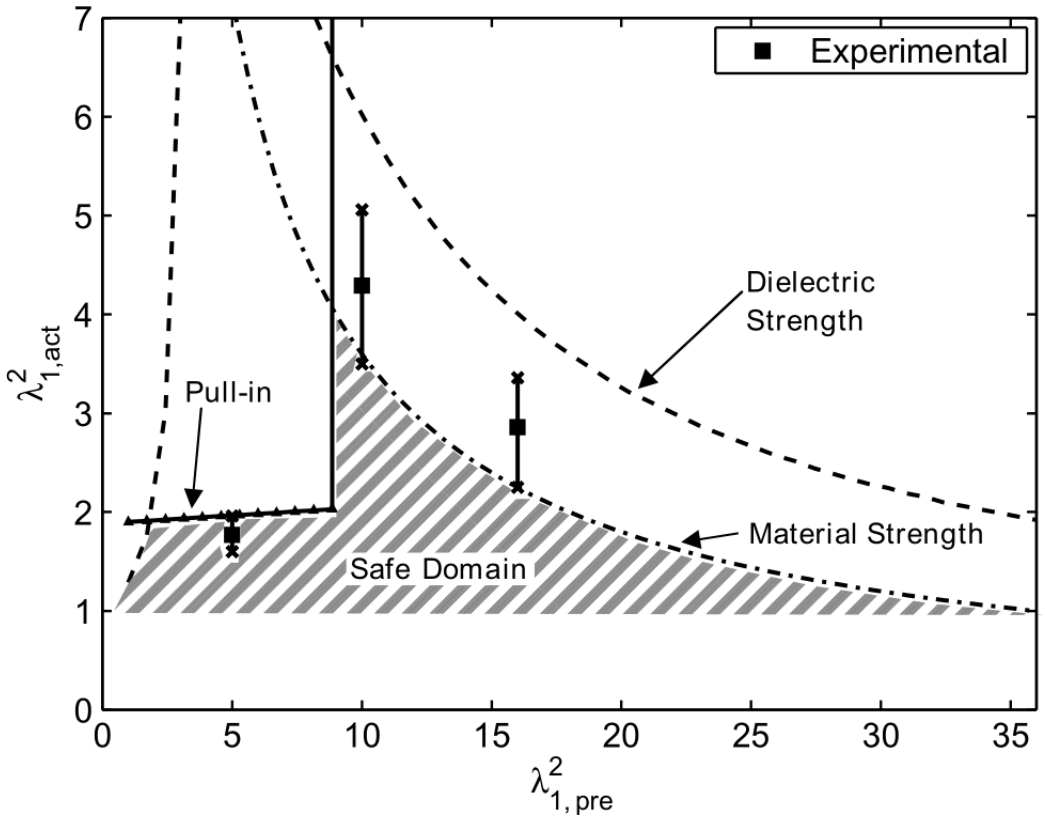

Figure 1.7.: Failure modes [2].

In summary, pre-stretching improves actuation performance because of the increase of breakdown strength. The effects of pre-stretch on the actuation properties of dielectric elastomer actuators have been investigated. However, a detailed analysis of the impact of pre-stretch on electromechanical coupling in dielectric elastomer actuator has not been presented. [9]

1.1.5. Electromagnetic force calculation

The forces acting on a DEA originate from the presence of electromagnetic fields. In this thesis two methods of calculating these forces are discussed. Firstly through the Maxwell stress tensor and secondly with Pelrine's equation.

1.1.5.1. Maxwell stress tensor

The Maxwell stress tensor couples the effects of electromagnetic fields to forces acting upon a body. It starts with Maxwell's equations. They are summed up below in the classical notation. [10]

First, Gauss's law:

$$\nabla \cdot E = \frac{1}{\varepsilon_0}\rho \tag{1.10}$$

Second:

$$\nabla \cdot B = 0 \tag{1.11}$$

Third, Faraday's law of induction:

$$\nabla \times E = -\frac{\partial B}{\partial t} \tag{1.12}$$

And fourth, Ampère's law with Maxwell correction:

$$\nabla \times B = \mu_0 J_f + \mu_0 \varepsilon_0 \frac{\partial D}{\partial t} \tag{1.13}$$

With E the electric field, B the magnetic field, D the displacement field, J_f the current density, ρ the total charge density, ε_0 the permittivity of free space and μ_0 the permeability of free space. Together with the force law $F = q(E + v \times B)$ they define Maxwell's Stress tensor as:

$$T_{maxwell} = \varepsilon_0(EE + c^2 BB - \frac{1}{2} I(E \cdot D + c^2 B \cdot B) \tag{1.14}$$

With c the speed of light and I the identity tensor which is [10]:

$$I = \begin{bmatrix} 1 & 0 & 0 \\ 0 & 1 & 0 \\ 0 & 0 & 1 \end{bmatrix} \tag{1.15}$$

The Maxwell stress tensor is a second rank tensor. Generally, a second ranAs noted above, DEAs are able to transduce mechanical energy and in order for that to be accomplished, the electrodes must typically stretch and contract with the polymer. Thus, the electrodes have to be compliant. The ideal structure of a DEA can be assumed as two electrodes with no resistance and an elastomer with an infinite resistance. The elastomer is furthermore assumed to be a perfect dielectric and to be perfectly elastic with no dissipative mechanical loses. With these assumptions, the electrical and mechanical aspects of the system are separately and together lossless in the sense that energy is conserved during the changes of state.k tensor is a linear mapping of a vector onto another vector. [11] In other words, when you would multiply a vector and a tensor, you would get a vector. Furthermore, a tensor, like a vector, is also built out of components. The components of the Maxwell stress tensor correspond to the components of the forces in the x, y and z directions in planes perpendicular to the x, y and z axises. Equation 1.16 shows a possible notation of the Maxwell tensor. The first indice refers to the plane perpendicular to that axis, the second indice refers to the direction.

$$T_{Maxwell} = \begin{bmatrix} \sigma_{xx} & \sigma_{xy} & \sigma_{xz} \\ \sigma_{yx} & \sigma_{yy} & \sigma_{yz} \\ \sigma_{zx} & \sigma_{zy} & \sigma_{zz} \end{bmatrix} \tag{1.16}$$

Fig. 1.8 shows a graphical representation of the components on an infinitesimal small cube. It should be noted that these components also act on the opposite faces, however in reversed direction.

The way the tensor is used specifically for the finite element model is described in sec. 3.2.5.

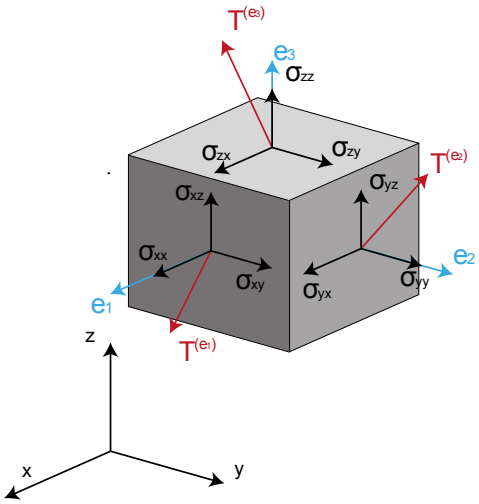

Figure 1.8.: Maxwell stress tensor components.

1.1.5.2. Pelrine's equation

Pelrine et al. [4] proprosed a simplified formula for DEAs, derived from the Maxwell tensor, to calculate the electrostatic pressure between two parallel plates. They assume that: "The elastomer has to have a uniform electrical charge distribution on infinitely large electrodes with uniform film thickness." The formula is given by:

$$p_{el} = \varepsilon_0 \varepsilon_r \left(\frac{U}{d}\right)^2 \tag{1.17}$$

With p_{el} the electrostatic pressure, ε_0 the permittivity in free space, ε_r the relative permittivity, U the electrode potential and d the elastomer thickness. This formula elegantly shows that the higher the relative permittivity is, the lower the voltage needs to be for the same electrostatic pressure.

1.1.6. Ogden model

There are many stress-strain models for hyperelastic materials but in this thesis the only one that will be used is Ogden's model based on the strain energy density. Several papers suggest Ogden as on of the best options to predict DEA behavior. [12, 13, 14, 15, 4] These models are needed because elastomer behavior is heavily nonlinear. Fig. 1.9 shows the difference in the stress-strain relationship of a metal (red) and an elastomer (blue). Note the linear part of the metal in the lower left corner.

The underlying concept of modelling the stress-strain relation is the deformation gradient. This gradient is again a tensor and is defined by two frames. First of all is the spatial frame or the physical space. Here, positions are represented by

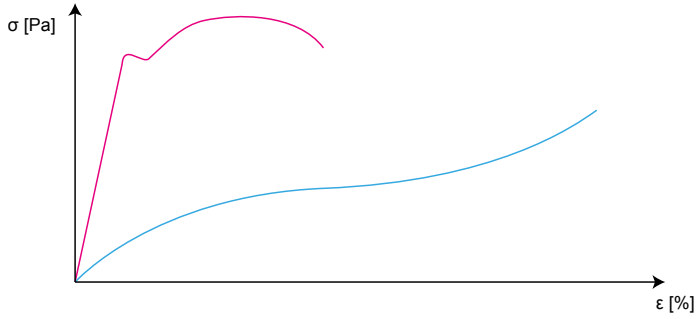

Figure 1.9.: Stress-strain relationships of a metal (red) and an elastomer (blue).

the lowercase spatial coordinate variables x, y and z. When the material deforms or moves, these variables will change with it accordingly. The second frame is the material or reference frame. This is denoted by the uppercase variables X, Y and Z. Each material particle will have a unique set of material frame coordinates. As they are reference coordinates, they don't change when the object moves or deformes. [16]

When a particle moves or deformes in time, the new coordinate is given by:

$$\bar{p} = \bar{p}(\bar{P}, t) = \bar{P} + \bar{u}(\bar{P}, t) \tag{1.18}$$

Where $\bar{p}(x, y, z)$ is a coordinate vector in the spatial frame, $\bar{P}(X, Y, Z)$ is a coordinate vector in the material frame and $\bar{u}$ is the deformation vector. In Comsol, the Cartesian components of $\bar{u}$ are u, v. Fig. 1.10 shows how the deformation vector is defined. $\bar{p}$

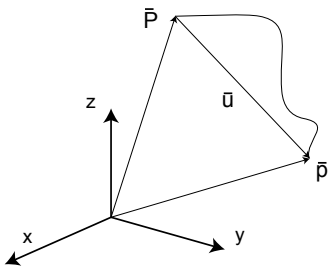

Figure 1.10.: Deformation vector.

The displacement vector only defines one point. A deformation field is able to define the deformation of every possible particle in a given material. Consequently, the deformation gradient is called F and is defined as:

$$F = \nabla \bar{u} = \begin{bmatrix} \frac{\partial u}{\partial X} & \frac{\partial u}{\partial Y} & \frac{\partial u}{\partial Z} \\ \frac{\partial v}{\partial X} & \frac{\partial v}{\partial Y} & \frac{\partial v}{\partial Z} \\ \frac{\partial w}{\partial X} & \frac{\partial w}{\partial Y} & \frac{\partial w}{\partial Z} \end{bmatrix} \tag{1.19}$$

In Comsol, the formulation is total Lagrangian. This means that the calculated strains and stresses are always in reference to the material frame [16].

Next comes Ogden's equation of strain energy density function. It is given by:

$$W = \sum_{i=1}^{n} \frac{\mu_i}{\alpha_i} (\lambda_1^{\alpha_i} + \lambda_2^{\alpha_i} + \lambda_3^{\alpha_i}) \tag{1.20}$$

With n, μ and α material constants and λ_1, $\lambda_2$and λ_3 the principal strains. The principle Cauchy stresses can now be calculated with:

$$\sigma_i = \lambda_i \frac{\partial W}{\partial \lambda_i} - p \tag{1.21}$$

With i one of the principle directions, λ_i one of the principle strains , W the strain energy density function and p a Langrange multiplier based on equation 1.2 [12].

1.1.7. Applicationsch

1.1.7.1. Artificial muscle

For last decades, biomimic actuators performing as artificial muscle have drawn much attention for compliant and lightweight robotic arms. [8] Also the performance requirements such as strain, actuation pressure, density, efficiency and speed of artificial muscle meet all the requirements of natural muscle. [17] Artificial muscles are able to mimic far more complex movements than the classic mechanical systems.

1.1.7.2. Generators

Dielectric elastomers also carry the ability of generating mechanical energy into electrical energy, therefore dielectric elastomer generators are being developed for both small-scale energy scavenging and large-scale energy generation. Unlike piezoceramics, the technology has the potential to harvest energy from ocean waves. Due to their large stretch rates DE's provide an excellent force coupling. Elastomers are highly stretchable, enabling excellent force coupling. These attributes may translate to lightweight, low-maintenance, and low-cost dielectric elastomer generators. [18]

2. Test setups

2.1. Sample preparation

2.1.1. Previous method

The current test sample is mounted by hand and is not very accurate. First, a piece of acrylic tape ($25\,mm$ by $25\,mm$) is pre-stretched by hand on a square plastic frame, as shown in Fig. 2.1. Afterwards, another square frame (copy of the first one) locks the elastomer film, ensuring it will stay in place. The next step is to isolate a circular section from the frame. This is done by clamping two rings above and underneath the frames. The ring is then cut loose from the outer frame and the edges are trimmed. Once the sample is ready the electrodes can be mounted by using silver evaporation or by applying carbon, as shown in Fig. 2.1. Finally, a high voltage generator supplies a voltage up to $12\,kV$ which can be applied to the electrodes. As shown in, two aluminum balls were used to make contact with the electrodes. By changing the amplitude of the voltage the actuation of the elastomer can be measured.

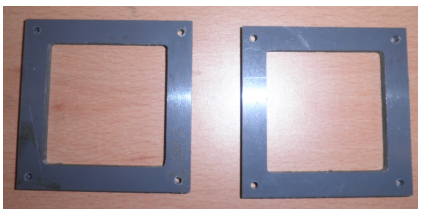

Figure 2.1.: Squares for pre-stretching.

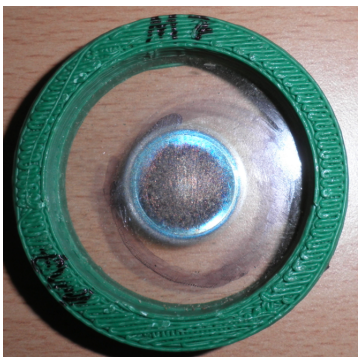

Figure 2.2.: Example of a DEA with silver electrodes.

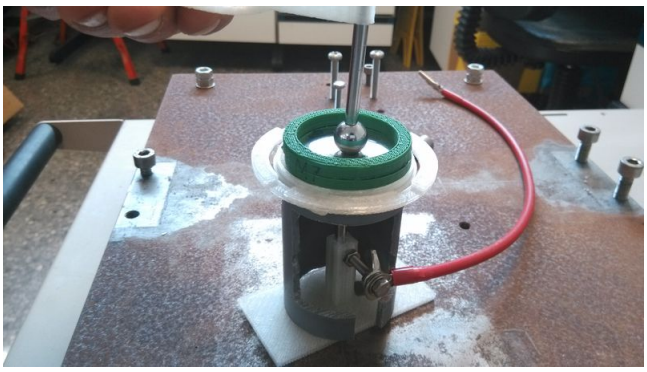

Figure 2.3.: The previous test setup.

2.1.2. Improvements

2.1.2.1. 3M VHB 4910 acrylic tape

The first step in the improvement of the sample preparation is to use a wider roll of the 3M VHB 4910 tape. Therefor, a roll with a length of $33\,m$, $50\,mm$ wide an $1\,mm$ thick was bought. So the role is twice as wide as the previous one, as shown in Fig. 2.4, and has the same length and thickness. Furthermore, it is assumed that the elastomer is a perfect dielectric and to be perfectly elastic, transducing its energy without dissipation of mechanical energy.

Figure 2.4.: The roll on the left is the one used in previous experiments and the roll on the right is the one used in the experiments handled in this paper.

2.1.2.2. Pre-stretch ratio

Pre-stretch is an important preparation for the experiment, due to the fact that it is able to significantly improve actuation performance. As the VHB tape is a hyperelastic material, the pre-stretch ratio can vary from a few percent up to 600 % [1]. In order to measure and control the pre-stretch ratio of the film, two dots are marked at a certain distance d_1 from each other. When the material is pre-stretched the enlarged distance d_2 is measured in between the dots, making it possible to determine the pre-stretch ratio by:

$$\lambda = \frac{d_1}{d_2} \tag{2.1}$$

It is clear that pre-stretch is an important preparation and that its ratio can have severe influences on the properties. Therefore, it is important that the tape is pre-stretched equally and that the ratio can be recovered.

Rubber ring Since all test samples will be circular, a rubber ring can be used to prepare the pre-stretched film for the sample. First of all a square piece from the VHB roll is cut and is pasted over a rubber ring. Then the areas outside of the ring are cut, to avoid accumulation. Next the ring has to be rolled inside out like a wrap, as shown in Fig. 2.5. Finally, the pre-stretched film can be clamped in between to rings. The downside of this method is that the material which is rolled up at the edge of the rubber ring is gone to waste. Unfortunately, it is not possible to prepare a pre-stretched samples with larger dimensions than the purchased item. In other words it is not possible to prepare a sample with a diameter larger than $50\,mm$, while other methods do provide this.

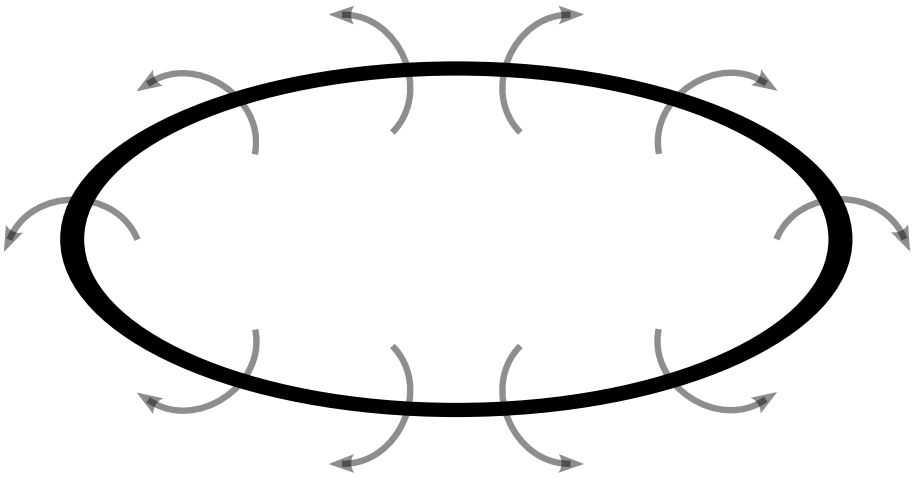

Figure 2.5.: The arrows in the figure show the way in which the rubber ring has to be rolled.

Diaphragma A diaphragma is a device mainly used in cameras to focus the picture at a certain distance, by increasing or decreasing the gap in the light track. It is possible to develop a diaphragm mechanism, on a scale comforting our working methods, in a fairly simple way. The working principle of a diaphragm is shown in Fig. 2.7. Fig comment: principle of a diaphragma.

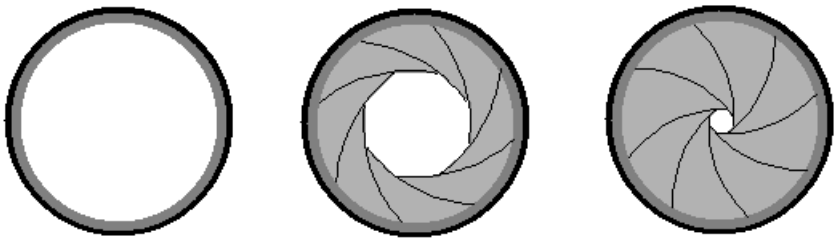

Figure 2.6.: Principle of a diaphragma.

The downside is that the metal plates, on which the elastomer will be sticking, will curl when the diaphragm is expanding. This causes undesirable twists in the tape.

Scissors mechanism The scissors mechanism is shown in Fig. 2.7 and more detailed drawings from the assembly and the individual parts can be found in Appendix sec. A.4. The plexiglass parts were made from a $700 \times 1000 \times 4\,mm$ plexiglass plate. They were constructed by a CNC milling machine and the use of AutoCAD (2007), Creatype (2007) and GPILOTE software. When the device expands, the nuts will experience a torque due to the friction with the washers and the plexiglass. A assential feature is that self-locking nuts were used to counteract the torque. These nuts are provided with rubber within the thread, as shown in Fig. 2.8, which counters the unscrewing of the nuts when they experience an external torque. As long as the counter torque from the self-locking nuts is higher than the torque created by the friction from the plexiglass and the washers, the nuts will stay in place.

The pre-stretch ratio is calculated by drawing two dots with an alcohol marker on the surface of elastomer. When the elastomer is pre-stretched the distance in between the two dots will incease, later the ratio can be recovered from Eq 2.1.

When a square piece ($50\,mm^2$) is cut off from the VHB roll and pasted on to the nuts of the device the red non-adhesive cover can be removed. Due to the self-adhesive properties, the VHB tape will remain stuck to the nuts during pre-stretch preparation. As the mechanism makes it hard to allow a simultaneous expansion in bi-directional way, a theoretical analysis of the degree of deformation is considered. The best way of approximating the degree of deformation in the x-plane, y-plane

Figure 2.7.: The scissors mechanism made from plexiglass.

and simultaneous xy-plane deformation are given by:

$$F_x = \begin{bmatrix} \lambda_{xx} & 0 & 0 \\ 0 & 1 & 0 \\ 0 & 0 & \lambda_{zz}^{-1} \end{bmatrix} \tag{2.2}$$

$$F_x = \begin{bmatrix} 1 & 0 & 0 \\ 0 & \lambda_{yy} & 0 \\ 0 & 0 & \lambda_{zz}^{-1} \end{bmatrix} \tag{2.3}$$

$$F_{xy} = \begin{bmatrix} \lambda_{xx} & 0 & 0 \\ 0 & \lambda_{yy} & 0 \\ 0 & 0 & \lambda_{zz}^{-2} \end{bmatrix} \tag{2.4}$$

In the present case and taking into account that the deformation of the VHB tape is done in a matter of minutes, no other parameters will have an influence on the deformation degree. The total degrees of deformation from non-simultaneous deformation in x-y and y-x order are

$$F_x F_y = F_y F_x \tag{2.5}$$

Figure 2.8.: Self-locking nut.

It can be concluded that, from a theoretical point of view, the deformation in simultaneous and non-simultaneous way can be considered equal.

This method was chosen above all others because it had the most advantages and was very simple in terms of construction.

2.1.2.3. Clamping the elastomer

Once the VHB tape is pre-stretched at the desirable level, it will be clamped in between two rings made out of plexiglass. This is exact the same operation as discussed in sec. 2.1.1 These rings have an outer diameter of $13\,mm$ and an inner diameter of $11\,mm$. 8 rings were made out of the leftovers from the plexiglass used to make the scissors mechanism, making it possible to work with several samples at the same time.

2.1.2.4. Electrode material and shape

Silver10 A thin film of silver can be planted on top of the elastomer by using an evaporation machine. The main working principle of such a machine can be seen in Fig. 2.9. First, a substrate is placed into the machine which creates a vacuum. This is necessary to avoid the formation of metal oxides like Ag_2O as these oxides have poor electrical conductivity. Then, the source material is evaporated by heat (thermal, electron-beam or resistive). The evaporated particles travel undisturbed to the substrate. After that, the particles condense onto the substrate, leaving a thin film deposition of the source material. [19] Finally, the substrate is taken out of the vacuum and is ready for further use. It should be noted that, the thickness of the electrode film can be controlled by the duration of the evaporation. And that the shape of the electrode can be achieved by using a mask.

Silver has excellent electrical properties but it is crucial that the electrodes are compliant and although only a thin film of silver is used. The relative high stiffness of the silver electrode will have severe influences on the range of actuation. mechanism

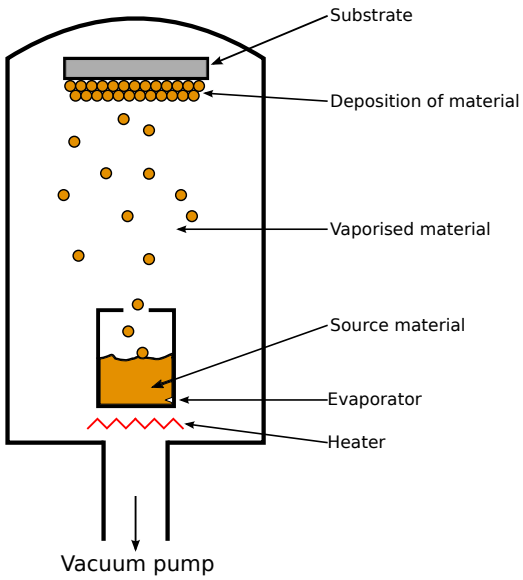

Figure 2.9.: Schematic drawing of a evaporation machine.

Carbon black The carbon black powder that is provided is carbon from the nodule stage and aggregate, so its particle size is within the range of 85 to 300 nm. [20] Due to the adhesive properties of the VHB tape the carbon black can be applied in a simple way by using a non-adhesive mask. As shown in Fig. 2.10, the mask is a negative of the circular electrodes. The basic concept of the mask is that it won't stick permanently to the film, this is why a mask was make from the material in which the VHB tape was packed.

Figure 2.10.: Mask used to paint the electrodes with carbon black. The gap has a diameter of 48 mm.

Time and strain rate have a significant impact on the resistance of the electrodes, causing a drop in the current. A downside is that the electrodes need more time to

reach their maximum charge as the strain rate increases. However the change in resistance can also be used for estimating the DEA deformation. [8] Although, carbon black has poor electrical conductive properties compared to silver, but the carbon black powder is chosen over the silver evaporation due to its excellent compliant properties.

2.1.2.5. Electrode shape

The shape of the electrode configuration is shown in Fig. 2.11. Previous studies made it clear that applying a relatively small circular electrode in the centre of the pre-stretched sample gave the best test results. [8, 21, 1, 2] The carbon black leading to the edges can be put in contact with an aluminum patch. On these aluminum patches the clamps of the high-voltage generator can be fixed. It is important to note that the aluminum patches make good contact with the carbon black electrodes, otherwise sparks may damage the sample.

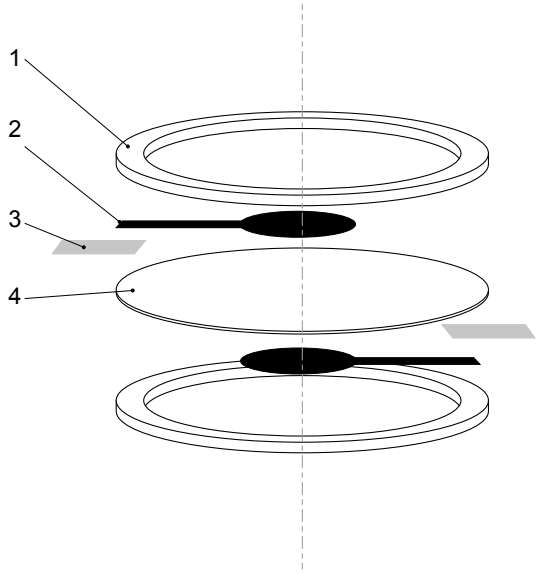

Figure 2.11.: The electrode configuration with: 1. Clamping rings. 2. Circular electrodes, with carbon tracks. 3. Aluminum connectors. 4. Dielectric membrane.

2.1.2.6. Summary

First of all, a square piece ($250\,mm^2$) from the VHB roll is cut and pasted on the scissors mechanism. Then, the non-adhesive red tape is removed and 2 dots are marked on the film using an alcohol marker. Next, the film is pre-stretched by expanding the scissors mechanism. Once the film is pre-stretched the distance is measured between the two dots. After this, we clamp the film in between two plexiglass rings, while doing this we have to apply the aluminum patches at both

sides of the film just over the edge of the inside perimeter of the ring. Finally, we can apply the mask and paint the electrodes on both sides of the sample. The result is a sample as shown if Fig. 2.12.

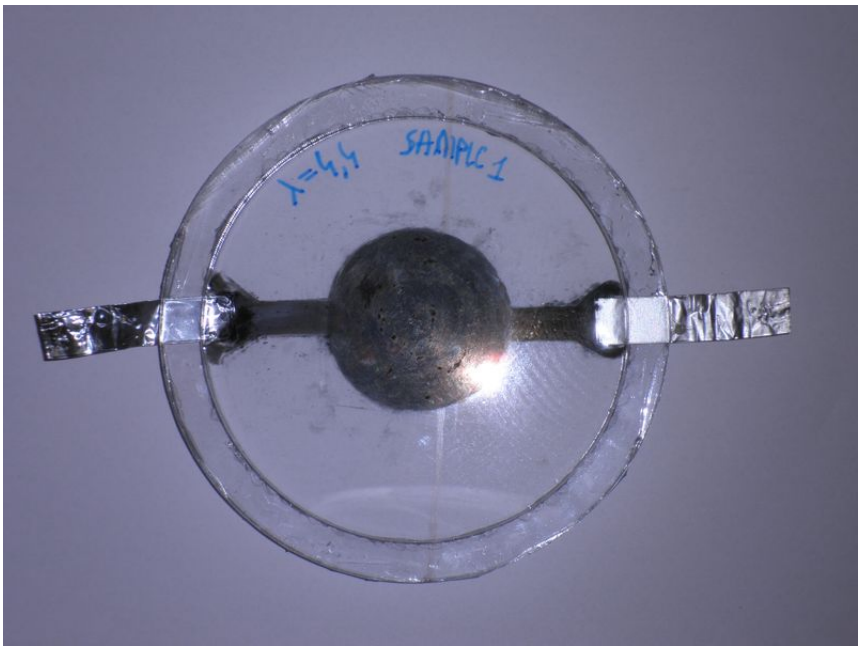

Figure 2.12.: Circular actuation sample with on the left side the aluminum patch for the upper electrode and at the right side the aluminum patch for the lower electrode.

2.2. Vibrometer

In this experiment, a laser Doppler vibrometer will measure the displacement of a DEA supplied with a voltage from 0 V to 4 kV.

2.2.1. Measurement principle

The vibrometers is designed to, among others, measure transient motion processes. The case here being the elastomer getting thinner. There are two main steps to measure the displacement. First, a high frequency laser signal is aimed an object. Secondly, the reflected light generate a frequency or phase modulation due to the Doppler effect. Demodulators in the processing unit (OFV-5000) can then extract the velocity and displacement.

Fig. 2.13 shows which displacement is measured.

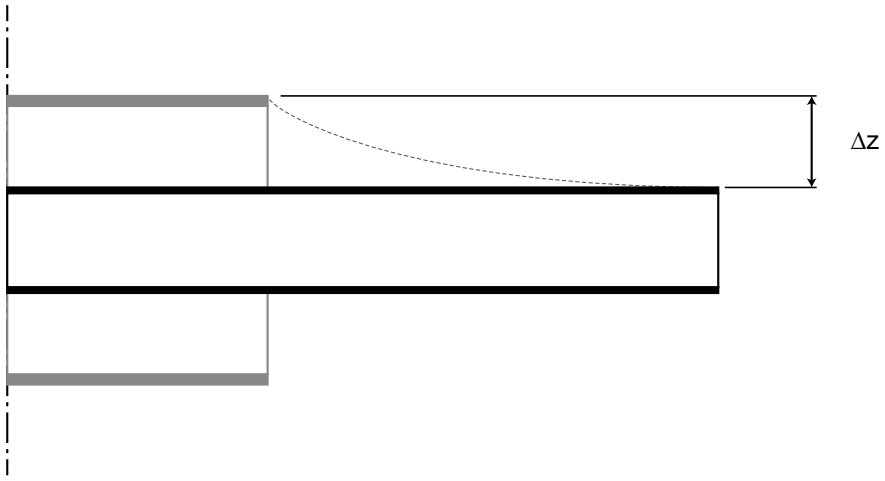

Figure 2.13.: Displacement measurement. The grey, thicker model represents the initial, unactuated state. The black, thinner model represents the actuated state.

2.2.2. Test setup

Fig. 2.14 shows the test setup.

The OFV-5000 generates an electrical signal that is proportional to the displacement. The possible resolutions range from 320 $\frac{\mu m}{V}$ to 80 $\frac{nm}{V}$. 80 $\frac{nm}{V}$ is chosen. An oscilloscope visualises this signal. The laser needs manual focus and there are two ways to control the signal strength: first by connecting the decoder to a beamer. The laser has an internally mounted camera which shows the laser dot. Second, there is a LED meter on the back of the laser which shows the signal strength as well.

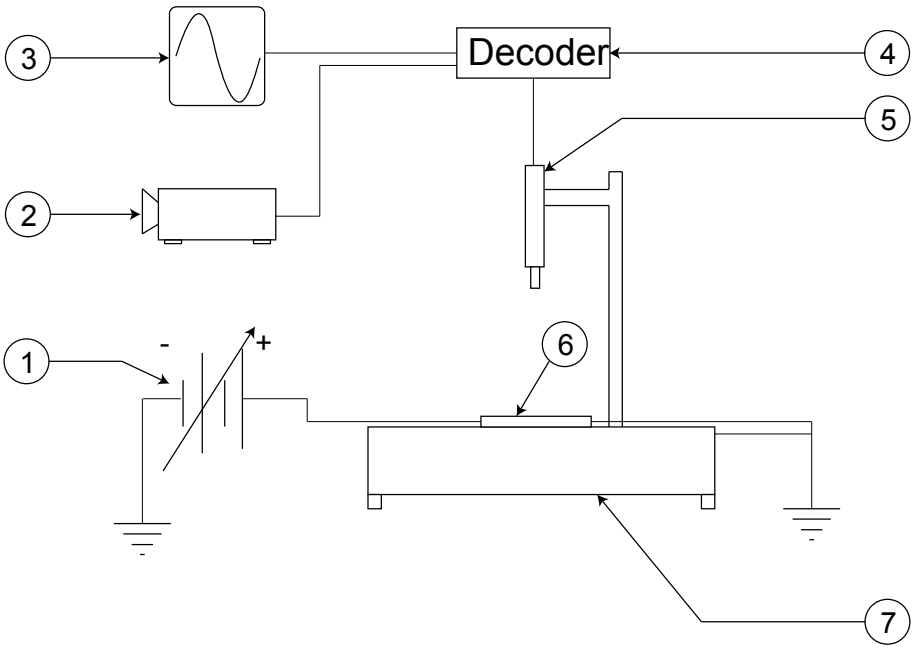

Figure 2.14.: The vibrometer setup. 1: DC voltage supply. 2: Projector. 3: Oscilloscope. 4: Decoder. 5: Mounted laser. 6: DEA. 7: Massive steel block.

The power source is a Spelman SL150 with a range from 0 to $150\,kV$. The voltage is applied on the top electrode. The current is set to $10\,mA$.

Since the vibrometer is very sensitive, the DEA must be isolated from external vibrations. The vibrometer even picked up transportation vehicles from the road nearby. In addition, it takes some time for the electrostatic forces and the internal forces of the elastomer to balance out, which opens up the possibility for more things to influence the measurement. One solution to counter this is a heavy block of solid steel (Fig. 2.14 Part 7) that serves as the basis of the test setup. This eventually reduced noise and improved signal strength.

2.2.3. Measurements

The experiment includes 25 measurements for a total of five samples. The voltage ranges from 0 to $4\,kV$ in steps of $0,5\,kV$. The measurements will be taken on different points at $10\,mm$ from the center of the electrodes.

Some areas are not fit for measurement. For example, areas that contain specks of carbon black. It is possible that if a speck lies on a radial line that the speck crosses the laser and thus influences the measurement. Furthermore, some areas have a thicker layer of carbon black and it is vital that the laser doesn't measure a transition of two regions with different electrode thickness. Fig. 2.15 shows the measurements on average. For raw data, see sec. A.8.

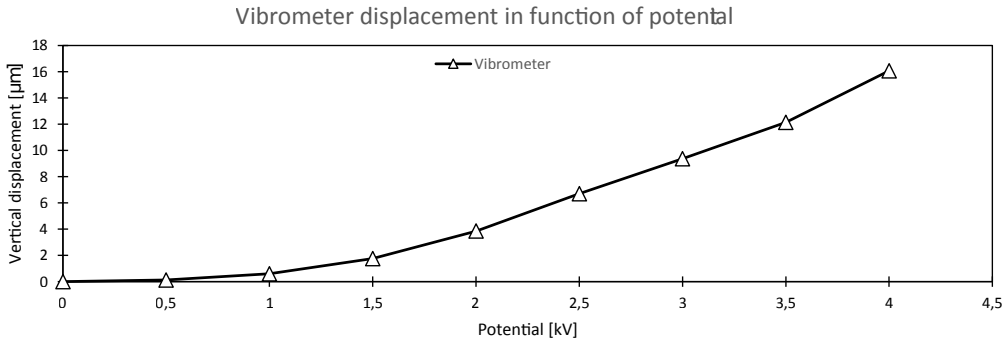

Figure 2.15.: Vibrometer results

2.3. Actuation measurement with videocamera

In this experiment, a digital camera will be used to determine the displacement of a DEA supplied with a voltage from $0\,kV$ up to $4\,kV$. It will not provide a high resolution measurement, but it will give good insights in what kind of displacement range might be expected.

2.3.1. Calculation methods

Due to the incompressibility of the elastomer, the volume in between the electrodes remains constant during actuation. Thus the next relation can be considered:

$$A_{in}d_{in} = A_{act}d_{act} \tag{2.6}$$

Furthermore, when the initial thickness of the film is calculated by using the pre stretch ratio, the thickness of the film in actuated condition can be determined by:

$$d_{act} = A_{in}\frac{d_{in}}{A_{act}} \tag{2.7}$$

As the shapes of the electrodes are circular, the surface can be calculated from the diameter of the electrodes:

$$A = \pi\frac{D^2}{4} \tag{2.8}$$

If Eq 2.8 is inserted in Eq 2.7 thickness in actuated condition can be determined by:

$$d_{act} = d_{in}\frac{D_{in}^2}{D_{act}^2} \tag{2.9}$$

In conclusion, from a theoretical point of view it should be possible to determine the displacement by monitoring the initial and actuated diameters of the electrodes.

2.3.2. Measurement error calculations

When only one measurement is carried out, the absolute error AE will be one division of the smallest unit found on the device. Considering this, the percentage error PE for a certain measurement will become [22, 23]:

$$PE(measure) = \frac{AE(measure)}{measure} 100\% \tag{2.10}$$

Furthermore, all measurement errors were calqulated with Eq 2.10 [23] and the following calculation rules:

$$AE(A + B) = AE(A) + AE(B) \tag{2.11}$$

$$AE(A - B) = AE(A) - AE(B) \tag{2.12}$$

$$PE(A \times B) = PE(A) \times PE(B) \tag{2.13}$$

$$PE(A/B) = PE(A)/PE(B) \tag{2.14}$$

2.3.3. Measurement principle

In this experiment a piece of millimeter paper will be used to measure the diameter of the electrodes. See Fig. 2.16. Since the millimeter paper is located $4\,mm$ underneath the sample (due to the rings which clamp the DEA), readings with the naked eye will give measurement errors. Therefore, a digital camera will be used to capture a picture which can be analysed later.

Furthermore, to eliminate the measurement error the camera should be placed as high as possible. Fig. 2.17 shows the improvement. Finally, with the help of correct zooming and focusing on the right area, a sharp image can be captured to measure the diameter of the electrode.

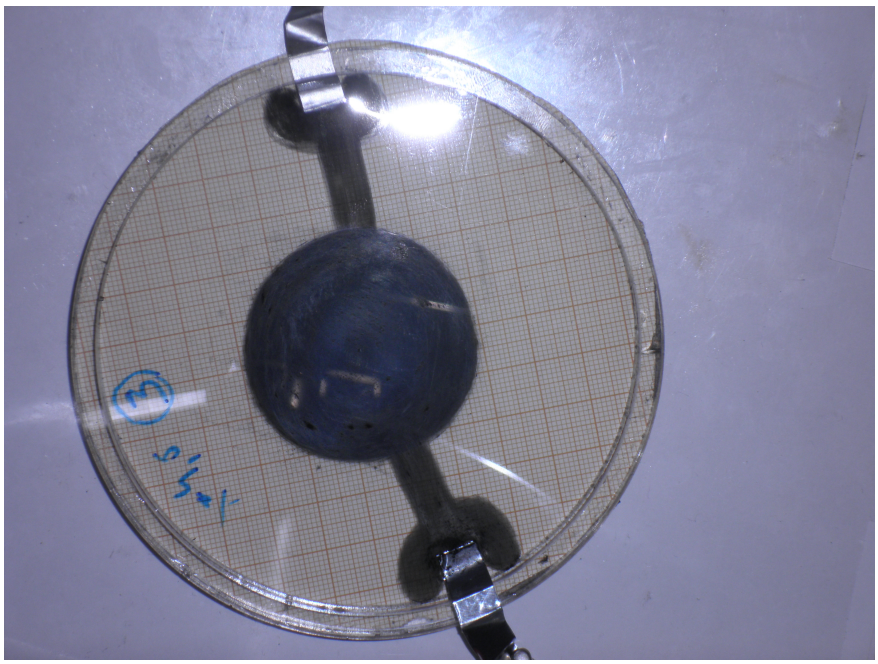

Figure 2.16.: Sample equipped with milimeter paper.

2.3.4. Test setup

The test setup can be seen in Fig. 2.18.

The power source is a Spelman SL150 with a range from 0 to 150 kV . The voltage is applied on the top electrode with a maximum current of 10 mA.

2.3.5. Measurements

For each of the five samples, two pictures are captured to determine the initial and actuated diameter of the electrode. By analyzing the pictures it turned out that the diameter of the DEA increased from 48 mm up to 53 mm, this is the average displacement of the all 5 samples. The results of the experiment can be found in Tab. 2.1.

Table 2.1.: Milimeter paper results

	0 kV	AE	4 kV	AE
$D\,[mm]$	48,0	1,0	53,0	1,0
$d\,[\mu m]$	52,0	5,1	42,7	5,1
$z\,[\mu m]$	0,0	/	9,4	1,5
$\frac{z}{2}\,[\mu m]$	0,0	/	4,7	0,75

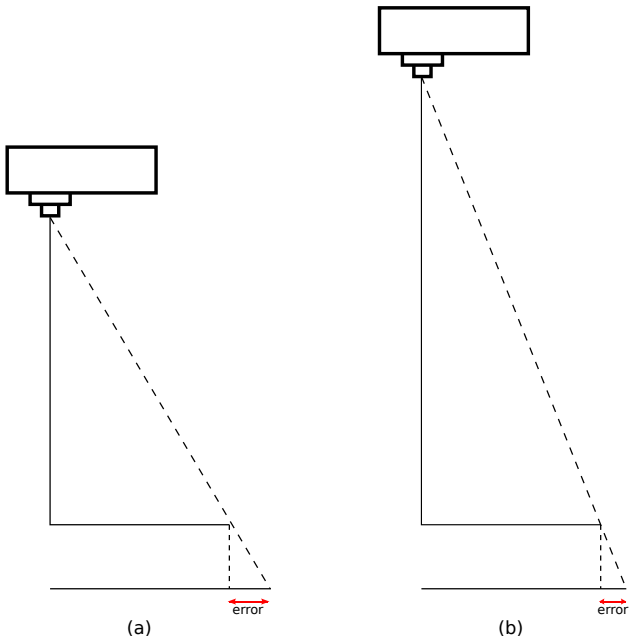

Figure 2.17.: The measurement error is reduced when the camera is placed at a higher level.

2.4. AC-voltage superimposition

Until now stretch sensors, spectroscopic analysis, cameras and lasers have been used to determine the state of the operating DEA. Instead of using these measurement tools to determine the initial state, strain or displacement of the sample, the DEA itself will be used as a sensor.

2.4.1. Theory

The best way of approximating a thin film parallel plate capacitor is:

$$C = \varepsilon_r \varepsilon_0 \frac{A}{d} \tag{2.15}$$

Where A is the surface of the parallel plate and d the distance between the two plates. When a voltage is applied, the electrodes squeeze the VHB film causing the surface to increase and the thickness to decrease. According to Eq 2.15 it is clear that the value of the capacitance undergoes a change during actuation as the numerator of Eq 2.15 increases and its denominator of decreases. Now the best way

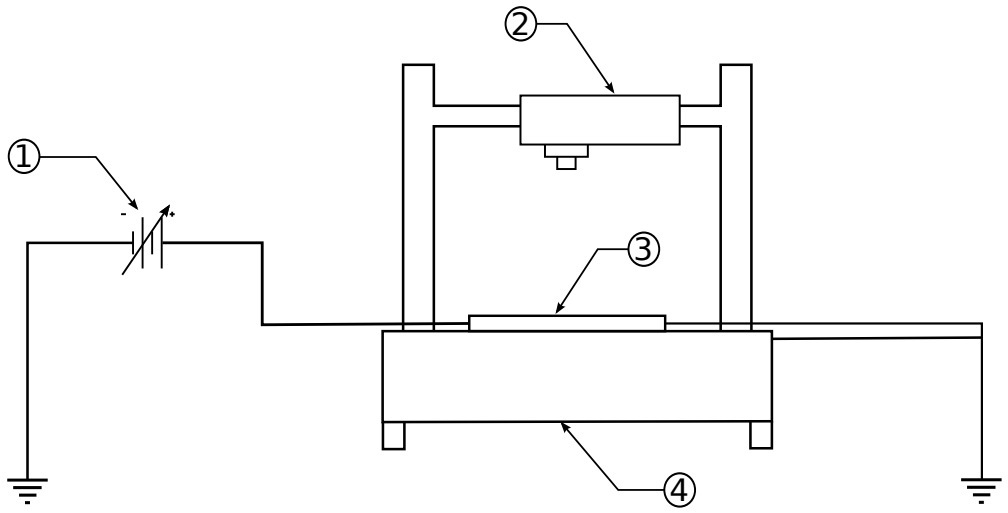

Figure 2.18.: 1: DC voltage supply. 2: Mounted camera. 3: DEA. 4: massive steel block.

to approximate the initial and actuated values of the capacitors can be determined by

$$C_{in} = \varepsilon_{r,in}\varepsilon_0 \frac{A_{in}}{d_{in}} \tag{2.16}$$

$$C_{act} = \varepsilon_{r,act}\varepsilon_0 \frac{A_{act}}{d_{act}} \tag{2.17}$$

Where C_{in} is the initial value and C_{act} is the actuated value of the capacitance. It is fair to assume that the dielectric constant (ε_r) remains constant during actuation, so:

$$\varepsilon_{r,in} = \varepsilon_{r,act} \tag{2.18}$$

Now Eq 2.16 and Eq 2.17 can be inserted in Eq 2.18

$$\frac{C_{in}d_{in}}{\varepsilon_0 A_{in}} = \frac{C_{act}d_{act}}{\varepsilon_0 A_{act}} \tag{2.19}$$

Furthermore, due to the incompressibility of the elastomer the volume of the elastomer in between the electrodes remains constant during actuation. This leads to the following relation:

$$A_{in}d_{in} = A_{act}d_{act} \tag{2.20}$$

If Eq 2.20 is inserted in Eq 2.19, the initial thickness can be obtained by

$$d_{act} = \sqrt{\frac{C_{in}}{C_{act}}} d_{in} \tag{2.21}$$

From a theoretical point of view, it should be possible to determine the thickness variation by measuring the values of the capacitance. Given that the initial thickness of the DEA can be determined by the pre-stretch ratio of the sample.

2.4.2. Test setup

Fig. 2.19 shows the experimental setup.

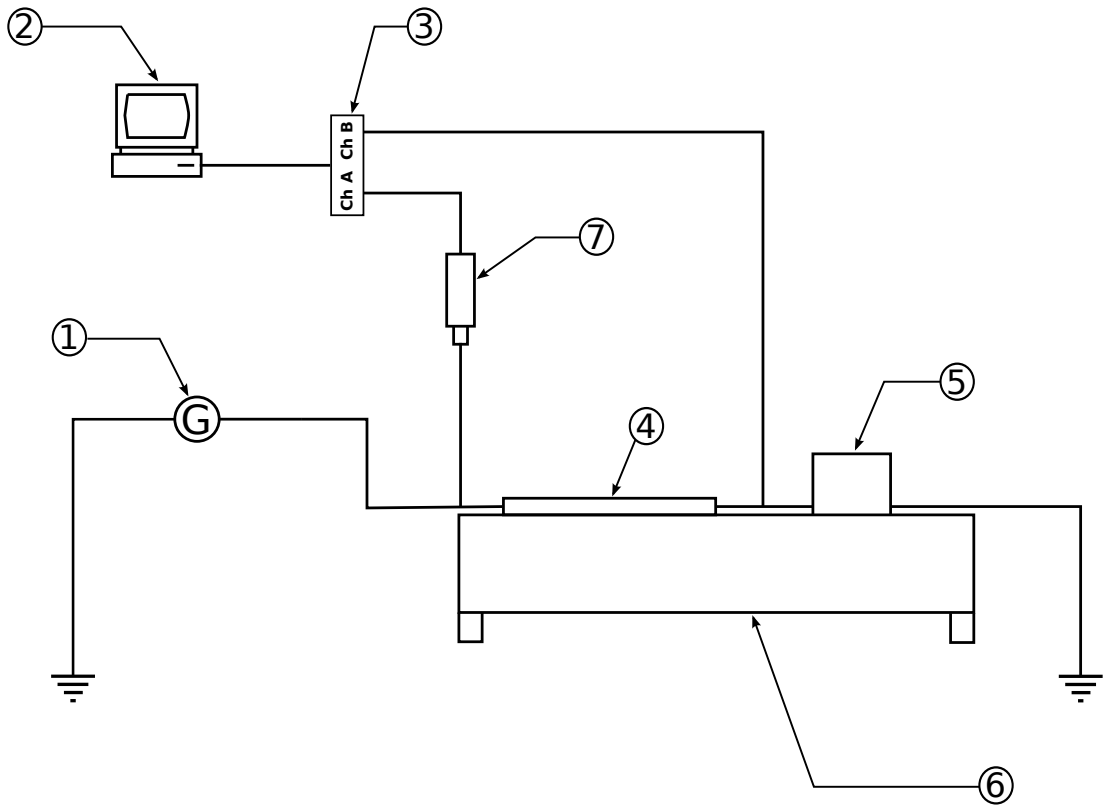

Figure 2.19.: 1: 20/30A and Techtronics generators. 2: PC. 3: Picoscope. 4: DEA. 5: $1\,kOhm$ resistance (EMC free cage). 6: Massive steel block. 7: High voltage probe.

2.4.2.1. Used devices

20/30A generator This device is able to generate a DC voltage up to $30\,kV$ and to add an AC voltage on its DC offset. This AC signal has to come from an external

generator. The voltage from the external generator is multiplied by 3000 before it is added to the DC offset voltage.

Tecktronics generator This generator is able to generate delta, sinus, block and saw-tooth waves with a peak to peak voltage from $50\,mV$ up to $4,00\,V$. And has a frequency range that expands from $1\,mHz$ up to $240\,MHz$.

Tecktronics P6015A high voltage probe The high voltage probe can measure high voltage values with the picoscope. The probe devides the voltage by a factor of 1000.

Picoscope 4235 The picoscope has 4 analogue inputs which are provided with a high voltage protection. Each channel has a resolution of 16 bits, a maximum sampling time of $80\,Msamples/s$. The data is transferred to a PC by USB interface.

Software The analogue values measured from the setup (current and voltage) are digitalized and converted to a CSV file. These files can be inserted in a excel document to make further calculations.

Resistance A $1\,k\Omega$ resistance was used to measure the current in the circuit, and was put in a EMC free area to reduce noise form other devices in the laboratory (especially generators). Finally, the entire test setup was placed in a Faraday cage to ensure safety.

2.4.3. Calculation methods

In the test setup two main values are measured: the applied voltage V generated by the two generators and the current I in the circuit. As shown in Fig. 2.20 channel A captures the voltage across the resistance of $1\,k\Omega$. Now, according to Ohm's law the current can be calculated. Fig. 2.20 also shows that channel B captures the voltage across the resistance and the capacitance (divided by a factor of 1000 due to the hight voltage probe). From the impedance triangle of a RC circuit, as shown in Fig. 2.20, the applied voltage can be recalculated from the current in the circuit and the impedance of the resistive and capacitive component. The applied voltage of the source should be equal to:

$$V_{source} = V_R + V_C \tag{2.22}$$

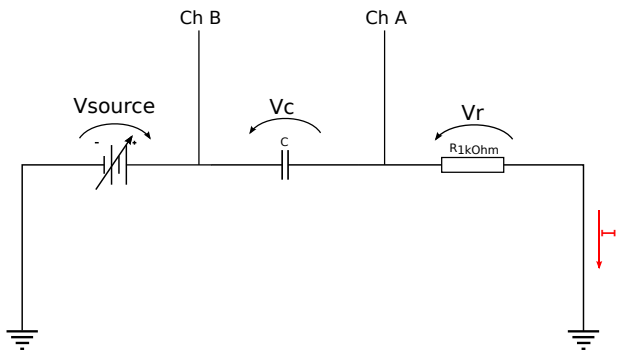

Figure 2.20.: Theoretical electrical scheme of the test setup.

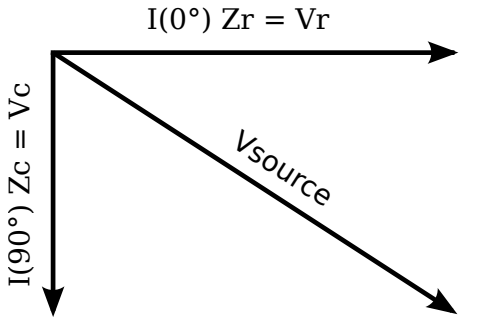

Figure 2.21.: Impedance triangle of a RC-circuit

$$V_{source} = I_{circuit}(\alpha)Z_c + I_{circuit}(\alpha + 90°)Z_r \tag{2.23}$$

As the software makes it possible to insert the data of the picoscope in Excel, the source voltage can be approximated by 2.23. For every applied frequency, 4000 samples were captured to approximate one period of the current and voltage in the circuit. If sample 1 is assumed to be the current at 0°, then automatically sample 1000 will be the current after a phase shift of 90°. By means of this there are no problems integrating Eq 2.23 in excel.

Finally, the values of the impedances are attained by iteration. In order to speed up the iteration a set of two equations can be solved. These two equations are nothing more than inserting the values of two samples in Eq 2.23. Later the value of the capacitance C can be calculated by

$$C = \frac{1}{j\varpi Z_c} \tag{2.24}$$

Appendix A shows an example of these calculations, allong with all the necessary explanations.

2.4.4. Measurements

A DC voltage from 0 up to $2,0\,kV$ will be applied to the sample, with steps of $0,5\,kV$. The maximum voltage in this test is limited untill $2,0\,kV$, this is due to the fact that the current within the circuit drops dramatically when the DC voltage is increased. In the end, above $3,0\,kV$, only noise is measured. Appendix B will give

more information. The sinusoidal AC signal, which is added to the DC voltage, has a peak to peak voltage of 150 V. The results of the tests can be found in Fig. 2.22 till Fig. 2.26. (The exact values of the capacitance and displacement can be found in Appendix sec. A.9)

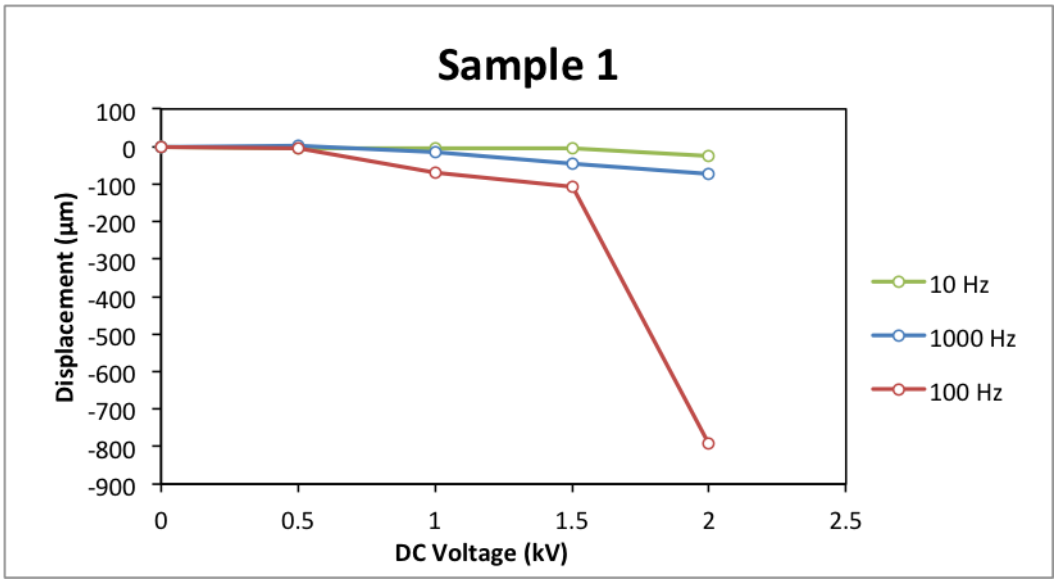

Figure 2.22.: Results of the AC superimposition experiment: Sample 1

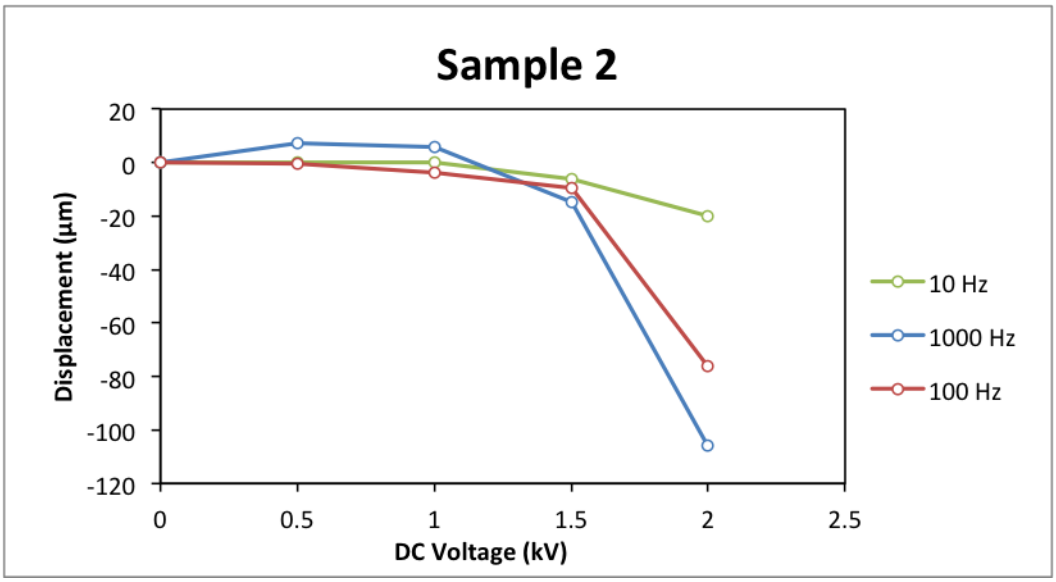

Figure 2.23.: Results of the AC superimposition experiment: Sample 2

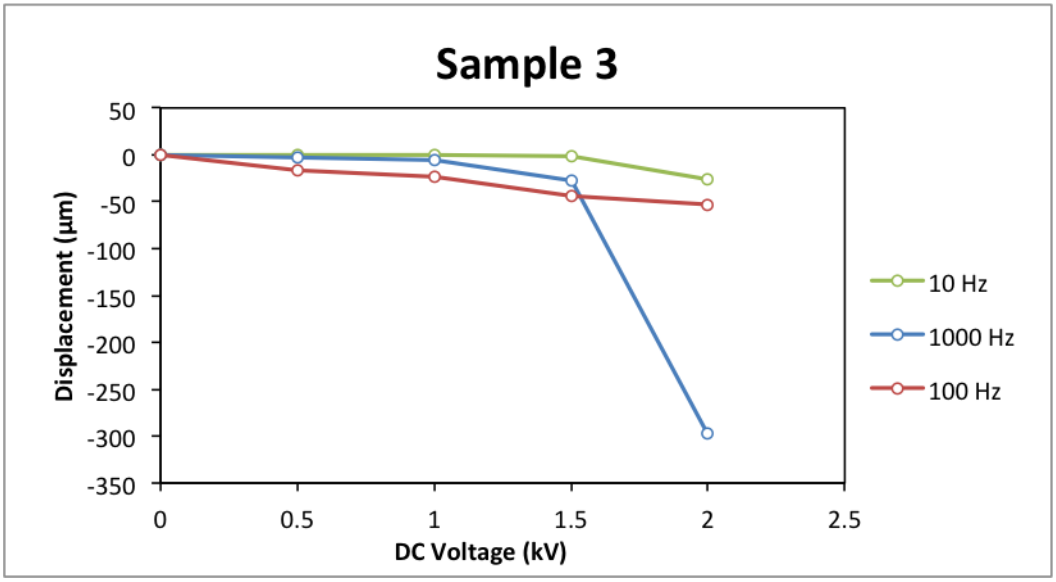

Figure 2.24.: Results of the AC superimposition experiment: Sample 3

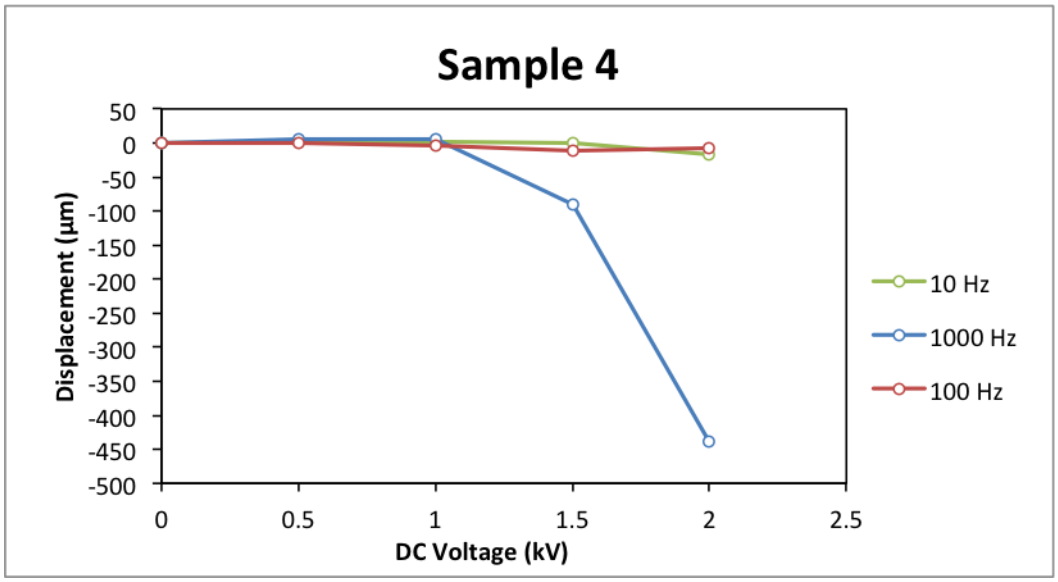

Figure 2.25.: Results of the AC superimposition experiment: Sample 4

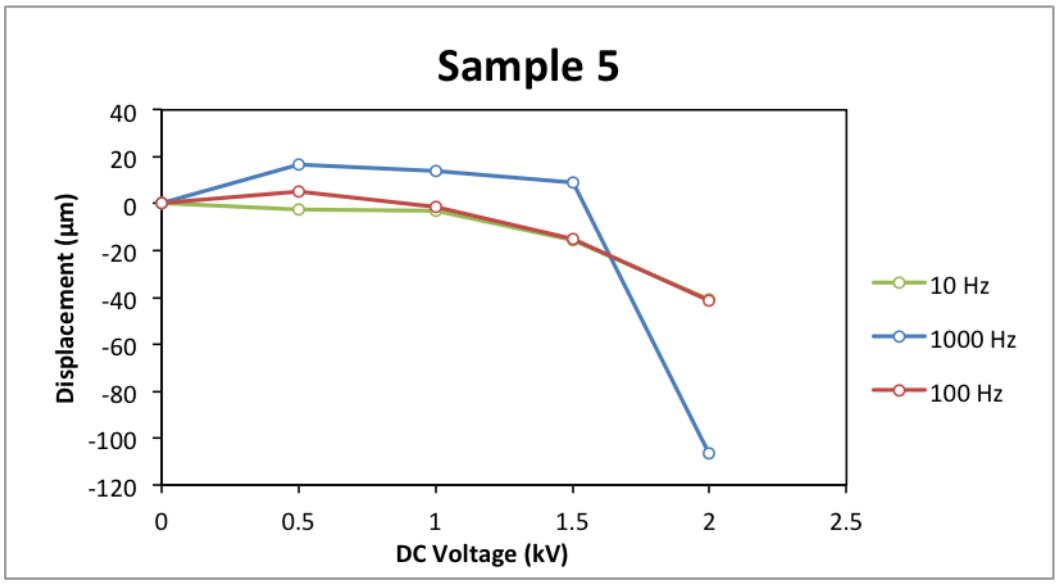

Figure 2.26.: Results of the AC superimposition experiment: Sample 5

3. Finite element model

3.1. Introduction

In this chapter, a finite element model is proposed in order to find a numerical solution of the actuation effects of the DEA using Comsol Multiphysics 4.3 First, a general idea of what the finite element method is and can do is given. Second, it is shown how the model is built and why certain assumptions have been made. Finally, the results are presented and compared to the experimental results.

3.1.1. Finite element method

A finite element method (FEM) tries to numerically solve a specific problem through the use of computer software. It has many applications in various in fields such as aerospace, chemical, biological and mechanical engineering because is has the capability to tackle complex geometries and material properties. Generally, there are three main steps in solving a finite element problem. First, the domain gets divived into smaller domains with a simpler geometry. This collection of smaller domains or elements is called the mesh. Second, sets of approximation equations are put on the elements. Whereas the problems were first of a differential nature, the equations are now transformed so they can be numerically approached. Third, the elements in the mesh are put into relation with each other. [24]

One thing to keep in mind is that the FEM still remains an approximation. There are a lot of different factors which will influence the accuracy of the result. One should always have an idea of how the result should look. FEM can then be used as a tool to verify expectations.

3.2. Model setup

Comsol has different physics modules that specialise in specific problems: e.g. heat transfers, acoustics and electromagnetic waves. These modules can be combined and in this model the solid mechanics and electrostatics modules will be used. The solid mechanics module takes care of the hyperelastic material, constraints and loads. The electrostatics module manages all the voltages and has the ability to calculate Maxwell forces. These forces can be used as parameters for a load in the solid mechanics module, thus coupling both modules.

3.2.1. Symbols

3.2.1.1. Constraints

Constraints put certain rules on mesh displacements. This is vital for the convergence of the model. Constraints and boundary conditions are narrowly connected. This model has three types of constraints. First of all, Fig. 3.1 is the symbol for the fixed constraint. This will set the displacements u and w to 0. These boundaries will stay fixed in space. In the physical model, this effect is created by the rings. They prevent the elastomer from moving. Second, Fig. 3.2 shows the symbol for symmetry. In the physical model this is the middle of the elastomer since both the upper and lower side are assumed identical. Lastly the axis of revolution is depicted as a dashed line on the left side of Fig. 3.4. This fixes only the u displacement.

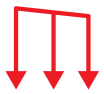

Figure 3.1.: Fixed symbol.

Figure 3.2.: Symmetry symbol.

3.2.1.2. Loads

Loads give points, boundaries or areas an external force or pressure. The input can be a number, a parameter or a variable. Fig. 3.3 shows the symbol. Here the module coupling takes place.

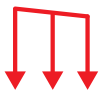

Figure 3.3.: Load symbol.

3.2.2. Geometry

There are different ways to model the actuator. Since there is a lot of symmetry and the actuator is circular, the primary choice is a 2D-axisymmetric model with an extra horizontal symmetry. An important remark is that the axes change from x, y and z, to r, φ and z, respectively. A 2D-axisymmetric model only calls for the calculation on a very thin slice, which simplifies the model and improves calculation time drastically. To get the result in the full three dimensions, the data can be mirrored about the r-axis and revolved around the z-axis.

An early proposal of the model is given by Fig. 3.4. The grey area is the elastomer and the transparent area is air. The model is also divided in a left section and a right section. The left section represents the part that is covered by the electrode. To simulate the effect of the electrostatic pressure, a boundary load constraint is put on this edge. To represent the plastic rings holding the elastomer in place, there is a fixed constraint at the end of the DEA.

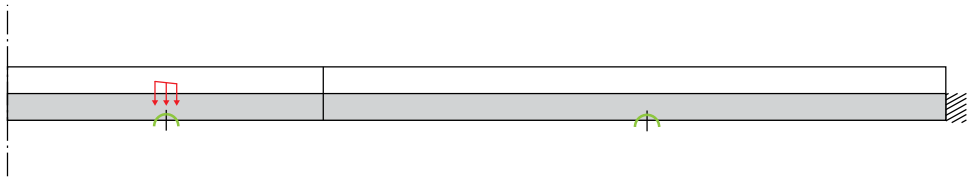

Figure 3.4.: 2D-axisymmetric Comsol model representation.

Although this model seems physically correct, it is not. If a force acts downward on the electrode, the elastomer has no other choice than to push radially outward since the elastomer is considered fully incompressible. But this effect gets obstructed by the right section of the DEA because it is fixed at the end. In reality, the section without electrodes absorbs the pushing motion of the actuated part by becoming thicker. It can do this 'absorbing' because of the pre-stretching. Imagine if the plastic rings wouldn't be there to hold the elastomer in place, then the elastomer relaxes and returns to its initial state. Thus, a better solution would be to remove the section on the right. This way, the model will better predict the actual actuation. Even better would be to model the internal forces in the right section, but that is out of the scope of this study. Fig. 3.5 shows the new model. Note that this model is without air. Early tests pointed out that the air did not contribute anything significant to the force calculation. The radius of the elastomer covered with electrodes is $24\,mm$.

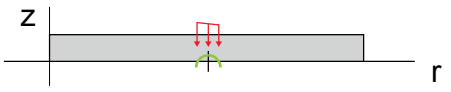

Figure 3.5.: Simplified 2D-axisymmetric Comsol model representation.

3.2.2.1. Elastomer thickness

Since no direct measuring devices to measure the thickness after pre-stretching were at hand, the thickness has to be calculated. There are two ways to do this. First, if the material is considered fully incompressible, the calculation of the thickness after stretching boils down to the following equation:

$$z_{pre-stretch} = z_{initial} \frac{1}{\lambda_x \lambda_y} \tag{3.1}$$

The stretch in the x and y directions are both $4,4$. Thus when $z_{initial} = 1\,mm$, $z_{pre-stretch}$ becomes $0,0517\,mm$. A second way is to let Comsol calculate the thickness itself. This is tested in sec. 3.3.1.

3.2.3. Material properties

This section covers the VHB 4910 elastomer material properties. Tab. 3.2.3 shows the relative permittivity ε_r, the Poisson's ratio ν and density ρ. The permittivity has been taken from [25] and the Poisson's ratio and density from the VHB data sheet. sec. A.3

Table 3.1.: Fixed elastomer material properties.

Material Parameter	Value	SI Unit
ε_r	4,7	
ν	0,49	
ρ	960	kg/m^3

Comsol offers different models to simulate hyperelastic materials. The three most used are the Neo-hookean, the Mooney-Rivlin and the Ogden models, but here only the Ogden model will be applied. [8, 3, 15, 26] all proposed parameter sets that differ from eachother. These variations arise from using different test setups and wether the elastomer is uniaxially or biaxially stretched . Here, a choice had to be made which set fits the DEA in this test the most accurately. The preference goes to Norris'.Tab. 3.2.3 shows the Ogden coefficients for this second order ($N = 2$) Ogden equation (1.20).

Table 3.2.: Ogden parameters.[3]

i	α_i	$\mu_i[Pa]$
1	1,450	112200
2	8,360	0,1045

Comsol leaves an option to choose whether the material is nearly incompressible or not nearly incompressible. When the option is selected, Comsol uses a total elastic energy function, composed out of the isochoric and volumetric strain energy density functions. [16] This is also called a mixed formulation. The governing parameter for this problem now becomes the bulk modulus K. It is one way to tackle the problem of locking. [27] states that: "Finite elements in solid mechanics are said to “lock” when exhibiting an unphysical response to deformation."

The bulk modulus indicates how incompressible a material is. 3M did not specify the bulk modulus directly, but it can be calculated from the Young's modulus E through the following formula:

$$K = \frac{E}{3(1-2\nu)} \tag{3.2}$$

With ν Poisson's ratio. Taken $E = 1,8\,MPa$ [28], $K = 30\,MPa$.

3.2.4. Terminal

By applying a terminal boundary condition, boundaries can have charges or potentials. The top boundary of the actuated domain gets a voltage of V_{top}. The bottom boundary gets half of this since it is supposed to be halfway of the ground electrode.

3.2.5. Electrostatic pressure

The electrostatic pressure will be linked to the model as a load constraint on the electrodes. There are two different ways to calculate the forces: the first one is to use the Pelrine equation given by:

$$p_{el} = \varepsilon_0 \varepsilon_r \left(\frac{U}{d}\right)^2 \tag{3.3}$$

The load component when modified for one half of the elastomer is given by:

$$P = \frac{1}{8}\varepsilon_0 \varepsilon_r \left(\frac{U}{z}\right)^2 \tag{3.4}$$

With P the electrostatic pressure on one side, ε_0 the permittivity in free space, ε_r the relative permittivity, U the total potential and z the height of one half of the elastomer. The second option is to use a Maxwell tensor component: the downward normal Maxwell pressure in the z direction or $es.dnTz$. es means that it is a parameter from the electrostatics module. It is also important to note that half of the Maxwell pressure is needed since it acts on one side.

3.2.6. Mesh

The mesh can be physics-constrolled or user-controller. A physics-controlled mesh is automatically generated and always consists of triangles. As the elastomer will become very thin and the mesh deforms with it, the mesh elements will become very narrow. Since the generated triangles generally have sharp corners, the stretching could cause corner angles to near zero degrees. This leads to a low quality mesh and possible inverted elements. A configuration which isn't optimal for good results. It is therefore better to use a mapped mesh which consist of rectangular elements. Fig. 3.6 shows this mesh. Because the model deforms mainly in the r direction, the corners will continue to stay at a right angle. Another advantage of a mapped mesh is that the structure can be precisely controlled. A built-in distribution function makes it possible to define the amount of elements on a certain boundary. The blue line is that defining boundary. In this image there are only 10 elements, but since the model will get thinner it is best to generate more elements.

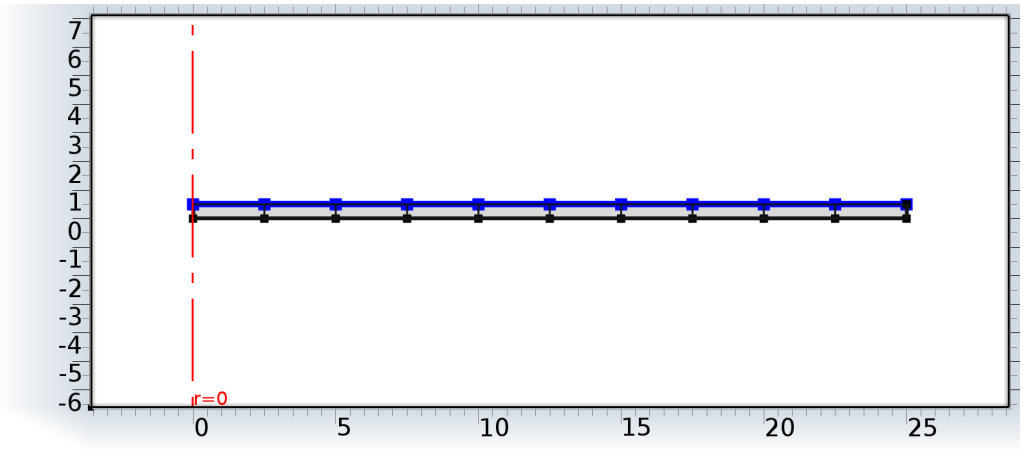

Figure 3.6.: Mesh of the pre-stretch model.

3.2.7. Other considerations

Firstly, this will be a stationary study, since only the actuated state in the end matters. This means that phenomena like viscoelasticity and fatigue are ignored. Second, to compute each value of a potential a continuation study is used. A continuation study will use the previous result as the initial state. In the continuation study the voltage is the changing parameter. It will go from $0\,V$ to $4000\,V$ in steps of $100\,V$. Third, since the mesh elements will become very narrow the geometry shape order needs to be set to lineair in order to avoid locking of the mesh, as higher order shape functions can't handle the low mesh element quality.

3.3. Calculations and results

3.3.1. Thickness

As stated in sec. 3.2.2.1, Comsol itself can be used to determine the elastomer's thickness after pre-stretching. A continuation study will gradually increase a radial force until the total radius reaches the stretched radius. The thickness is then extracted through point measurements. In order to do this, the model needs to be adapted for radial stretching. Fig. 3.7 shows this model. It starts off with a radius of $25\,mm$ and is stretched until a radius of $110\,mm$ has been reached. This corresponds with a pre-stretching ratio of $\lambda = 4,4$. The model is also 2D-axisymmetric with an extra horizontal symmetry condition. An outward radial force at the right edge elongates the elastomer thus making it thinner.

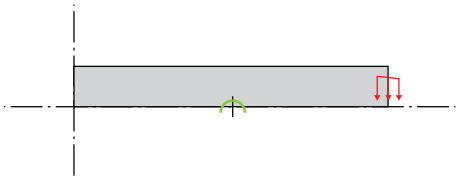

Figure 3.7.: Comsol pre-stretch model.

Fig. 3.8 shows the thickness in function of the radius. At $110\,mm$ it shows that the thickness is $0,0265\,mm$.

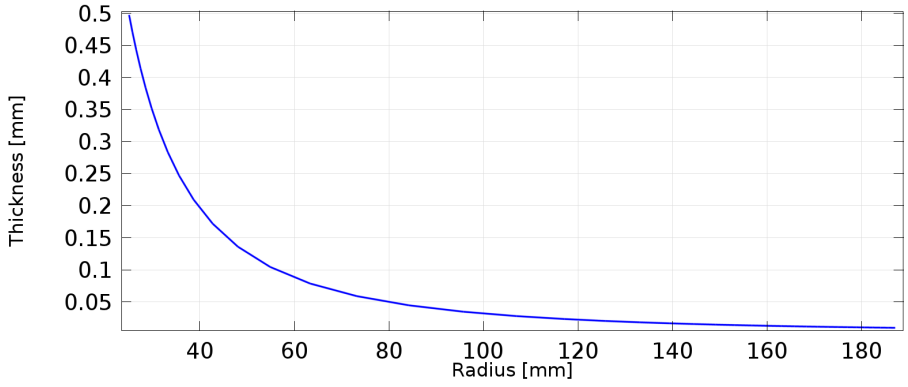

Figure 3.8.: Thickness in function of radius.

This way the total thickness will be $z_{pre-stretch} = 0,053\,mm$. This is close to the result calculted from 3.1.

3.3.2. Actuation

First of all is the thickness in function of the voltage. Here the thickness is taken from the Comsol calculation. Fig. 3.9 shows the result.

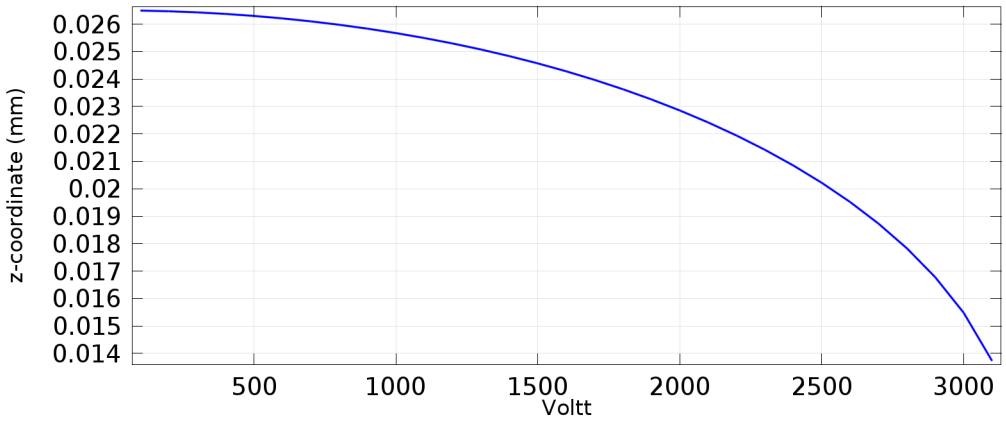

Figure 3.9.: Thickness in function of voltage.

The thickness decreases in a nonlinear fashion until $3100\,V$. Here, the electrostatic field is strong enought that the elastomer collapses. This is also called material breakdown. The values of thickness decrease per $500\,V$ are given by the following table:

Table 3.3.: Finite element model displacement.

$U\,[kV]$	$\triangle d\,[\mu m]$
0	0
0,5	0,20
1,0	0,83
1,5	1,93
2,0	3,65
2,5	6,65
3,0	11

Second is the electrostatic pressures graph. Fig. 3.10 shows both the electrostatic pressure from the Pelrine equation as the downward normal Maxwel z tensor. The pressures overlap very well.

Lastly are the convergence plot of the iterations, seen in Fig. 3.11. Generally there is a fast and clean convergence.. The total calculation time was 8 seconds.

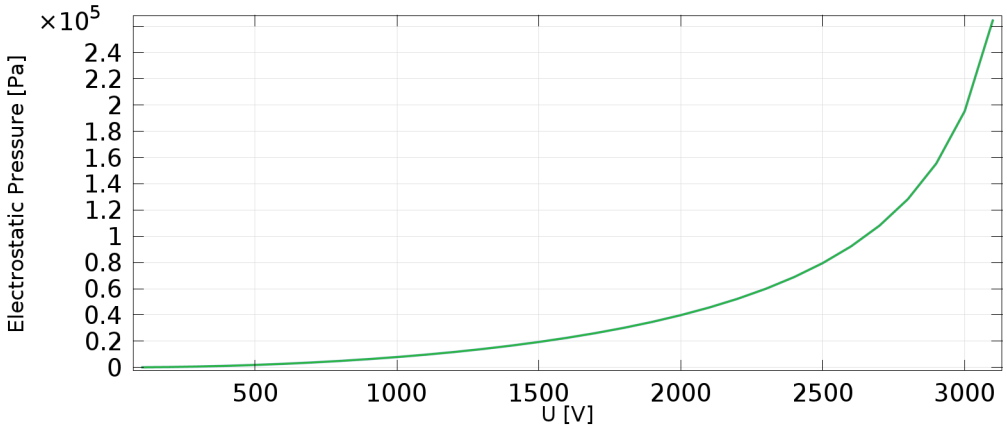

6.28

Figure 3.10.: Electrostatic pressures (overlapping) in function of voltage.

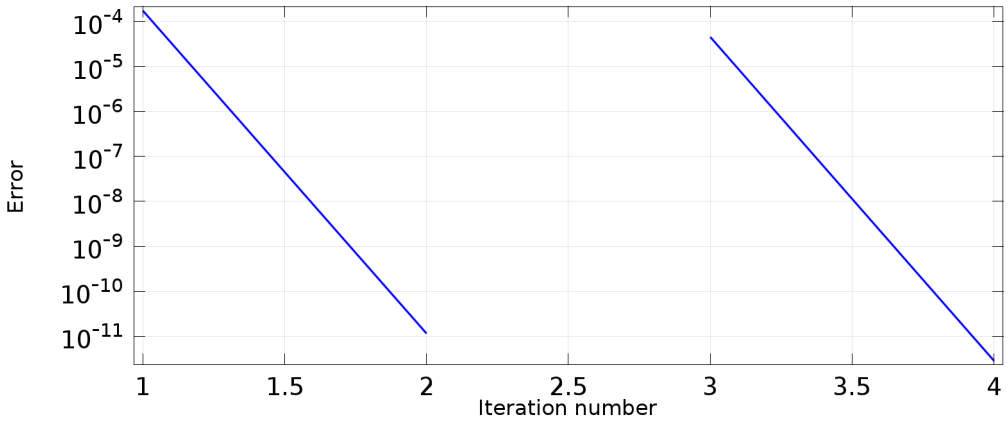

Figure 3.11.: Convergence plot.

3.4. Comparison

Fig. 3.12 shows the results of the laser vibrometer from sec. 2.2.3 and the finite element model. Both displacements account for one side of the elastomer. In order to get the full displacement the results need to be doubled. Tab. 3.4 gives the numerical values.

Up until $2,5\,kV$ the model follows the experimental data well. From then on, the Comsol model begins to deviate from the vibrometer results. At $3\,kV$ the FEM displacement is 18 % more than experiment displacement. The FEM went as far as $3,195\,kV$ (not shown), which is until material breakdown. However, the fabricated DEAs did not show any signs of breakdown up until $8\,kV$ or more. The actuation difference might be because of the carbon black. Irregularities can cause more resistant concentrations and slightl variations in thickness. Consquently, this results in an unevenly distributed electrostatic field. Therefor inhibiting the actuation partly. On the other hand, since the Ogden parameters are taken from another paper. The parameters might not fully reflect this DEA design.

The carbon black distribution problem could be solved using a different technique of applying the substance. A possible solution could be a stamp which is covered with carbon black and afterwards made smooth to create an homogenous layer. Another solution could be a roller that applies a certain amount of carbon black with each revolution. One could also replace the carbon black entirely. Ideally combining the conductivity of silver with the compliance of the carbon black. Some techniques include thin copper wires or ion-implanted electrodes. [2, 29]

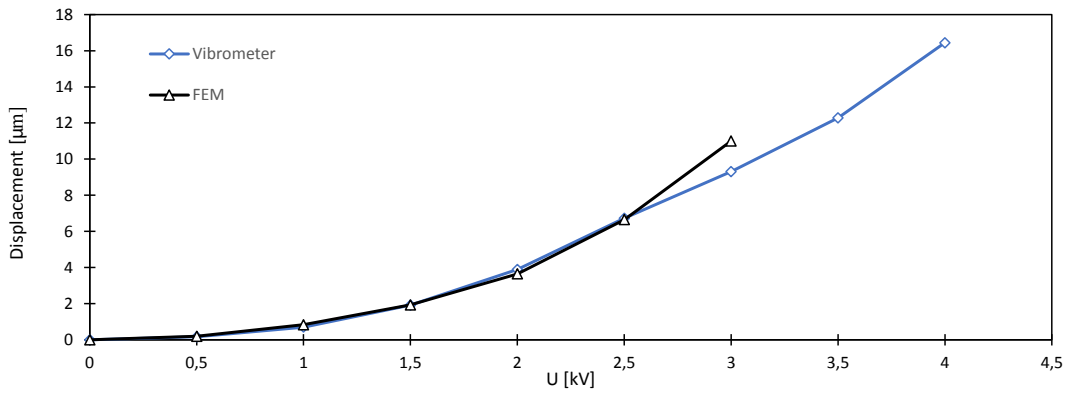

Figure 3.12.: Vibrometer and Comsol results

Table 3.4.: Displacement comparison between the vibrometer and FEM.

$U\,[kV]$	$\triangle d_{FEM}\,[\mu m]$	$\triangle d_{Vibrometer}\,[\mu m]$	Error [%]
0	0	0	0
0,5	0,20	0,17	16
1,0	0,83	0,70	18
1,5	1,93	1,91	1
2,0	3,65	3,90	6
2,5	6,65	6,73	1
3,0	11	9,31	18
3,5		12,28	
4,0		16,44	

4. Conclusions and future work

4.0.1. Conclusions

4.0.1.1. Digital camera

First of all there is no doubt that the experiment done with the digital camera is the most trustworthy. Despite a final error of 16% ($\frac{0,75}{4,7}$), see Tab. 2.1, the experiment provides a good guideline of what to expect in other setups. Finally, the measurement error of the test makes it possible to determine the thresholds, 4,0 μm and 5,4 μm, of the final displacement at 4,0 kV, which cannot be exceeded.

4.0.1.2. Vibrometer

When the results from the vibrometer are compared with those of the digital camera, it is clear that they don't coincide to one another. Fig. 4.1 shows the thresholds of the video camera included within the results of the vibrometer results. It also shows that the final displacement, detected with the vibrometer, still deviates with a factor 3-4 compared with the displacement detected by the video camera. And all of this despite the vibrometers high resolution, see appendix sec. A.5.

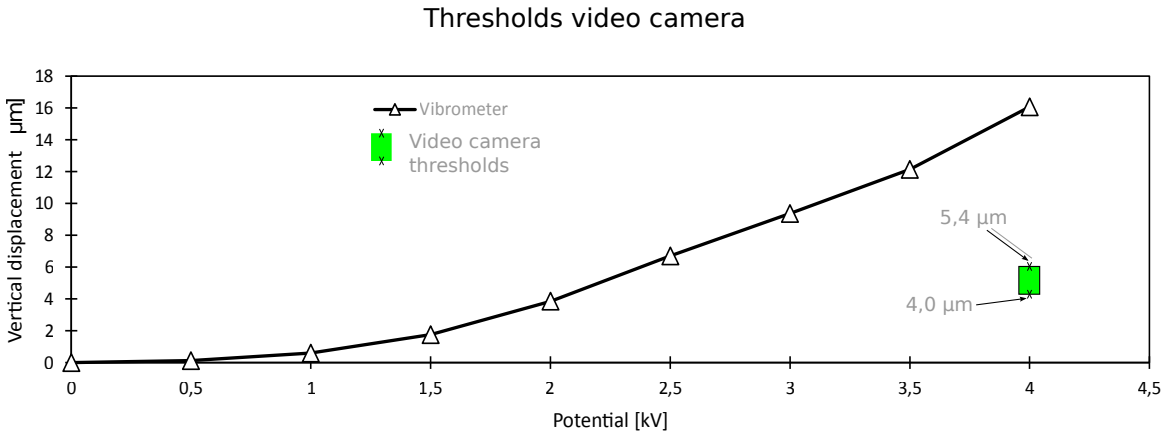

Figure 4.1.: The green area shows the thresholds of the video camera, this is the range in which the final displacement of the samples should be located.

It could be possible that, during actuation, not only the thickness of the elastomer decreases but also the thickness of the electrodes. Since the DEA keeps on actuating

at high voltage, the electrodes have to remain conductive. This can only be achieved if the particle formation of the carbon in the electrodes is rearranged, to make sure that electric conductivity is retained. Hereby it is highly acceptable that the thickness of the electrodes will decrease, as the surface of the electrodes increase during actuation. All in one, it is fair to assume that the vibrometer detected the displacement of the elastomer and on top of that, also the displacement of the carbon electrode. Fig. 4.2 shows the total displacement measured by the vibrometer.

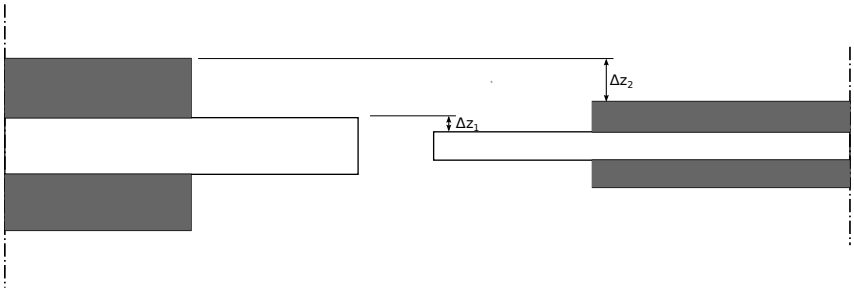

Figure 4.2.: The grey areas are the electrodes and the white space in between them is the elastomer. $\triangle z_1$is the actual displacement of the elastomer and $\triangle z_2$ is the displacement of the electrodes summed up with the actual displacement of the DEA.

4.0.1.3. AC-voltage superimposition

It is clear that it is not possible to measure the capacitance of the sample. As can be seen in the graphics of the test results in sec. 2.4.4, the curves are too far separated from each other. Therefore, it would be pointless to make an average of these measurements as the shape and gradient of every test is different.

A possible explanation could be that there are parasitic components (resistive, capacitive and inductive) in the circuit, which have a severe influence on the measured capacitance. Fig. 4.3 shows the electrical sceme with the parasitic components such as the resistance of the carbon tracks and the parasitic capacitance within the high-voltage probe. The parasitic components of the Picoscope are not integrated in the sceme, due to their minor influence in comparison to the high voltage probe.

4.0.2. Future work

4.0.2.1. Vibrometer

A vibrometer is an excellent and frequently used device to measure very small displacement, such as the once described in this paper. Most laboratory facilities own or are familiar with such a device, this is why it is a promising device to detect the displacement of DEAs.

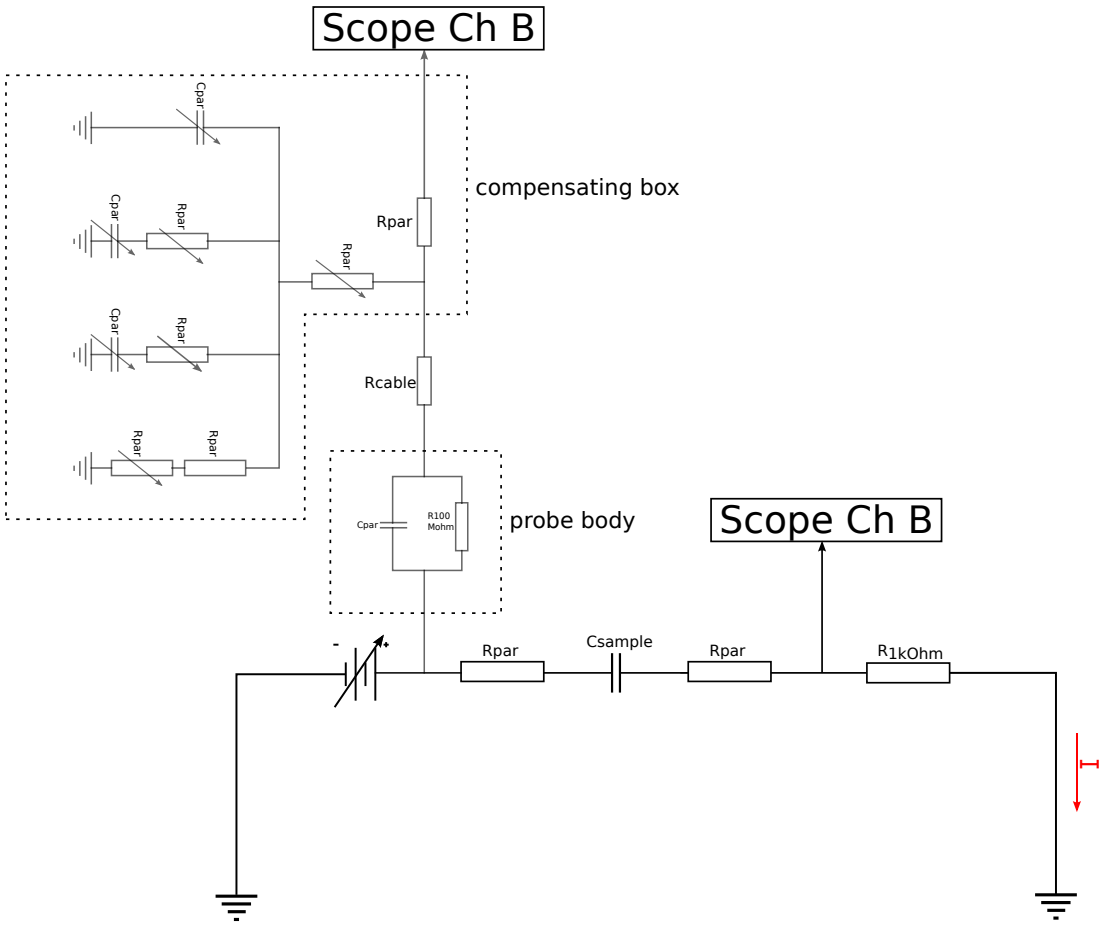

Figure 4.3.: Electrical scheme with parasitic components.

As the vibrometer setup in sec. 2.2 gave disappointing results, due to the fact that the thickness of the electrode changes during actuation. In order to eliminate this phenomenon, another configuration of the carbon black electrodes could be investigated. In particular, the shape of the electrode will be the exact negative of the one investigated in this work, the new shape can be seen in Fig. 4.4. The plain area in the middle of the sample will become the area where measurements will be made. Even though this area is plain, the vibrometer has no problems detecting small changes of displacement. Furthermore, the connection to the electrodes can be placed at the edge of the sample, eliminating the need of carbon tracks.

Finally, it should be noted that the thickness of the elastomer in the middle will increase, due to the fact that the sample is pre-stretched. Most likely, a new FEM model will have to be made to better understand what happens when a high voltage is applied to the new configuration.

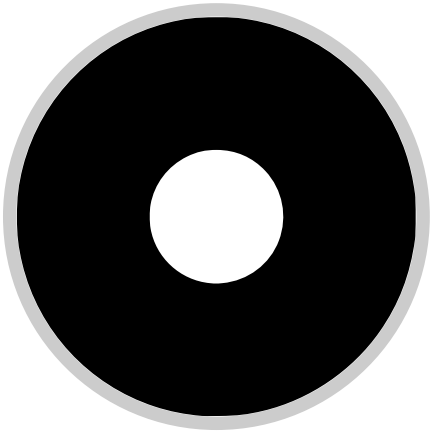

Figure 4.4.: The new sample configuration, the black area is where the electrodes are pasted.

4.0.2.2. AC voltage superimposition

Analyzing the displacement of DEAs with the aid of video analysis and with a vibrometer will satisfy research facilities and schools. But when applications will be designed, the displacement will be required in real time, as today's systems all work with the aid of digital feedback systems.

Since the parasitic capacities of the experiment of the setup in Fig. 4.5 contaminated the electric circuit, making it impossible to measure the capacity. However, when the total capacity of the DEA is increased significantly the parasitic capacities could be neglected from the circuit in Fig. 4.3. This can be achieved by connecting several DEAs (all with the same dimensions) parallel to each other, as parallel placed capacities can be simply summed up. Fig. 4.5 shows the electrical sceme of such an improvement. Finally, by using shielded cables and working in an EMC free environment, noise within the signals will be reduced, making it possible to calculate the value of capacity more precisely.

4.0.2.3. Digital videocamera

By using a digital video camera it could be possible to analyze the actuation of the DEA in real time. By means of this other aspects of DEA properties can be investigated, such as the time lag of the actuation and the stretch ratio at the moment when breakdown occurs, could be examined more precisely.

4.0.2.4. Conductive rubber

It is hard to achieve a uniform distribution of carbon when a DEA is constructed, therefor a carbon incorporated elastomer could provide great results. Moreover, the

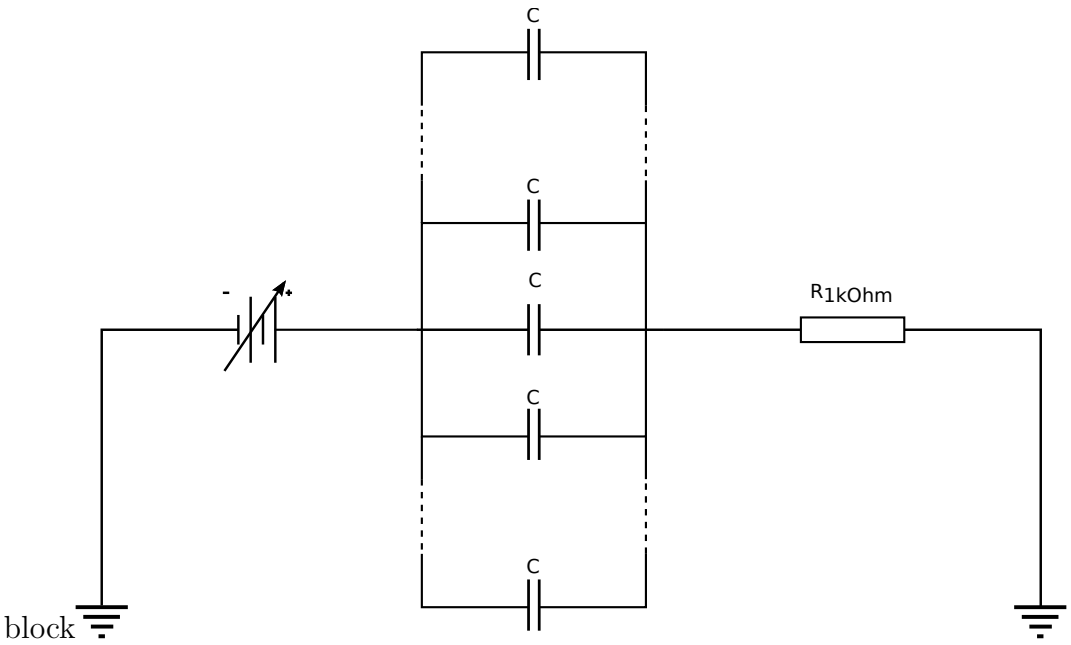

Figure 4.5.: The number of capacities has to be determined from the parasitic capacities of the measurement equipement.

elastomer, used to incorporate the carbon black, can be made of the same material as the dielectric membrane in between them [30]. Now the composition of these two elements can be considered as an incompressible material and the Young's modulus wil be as good as the same.

A. Appendix

A.1. Peak current (AC superimposition setup)

Before the actual experiments of measuring the capacitance, it is obvious some other tests on the sample were done as well. An example is the breakdown voltage. Another of those tests was measuring the peak current from in the circuit according to the applied DC voltage. Although the total capacity increases, the total current decreases because of the resistance variation of the graphite electrode.

A.1.1. Results

As shown in Fig. A.1 it is clear that the peak current drops dramatically after $2,0\,kV$. As the current becomes very low, the test setup becomes very fragile to EMC contamination (although we put the resistance in a cage of Faraday). This is why the tests for calculating the capacitance were done with a DC voltage from $0\,kV$ up to $2,0\,kV$ with steps of $0,5\,kV$.

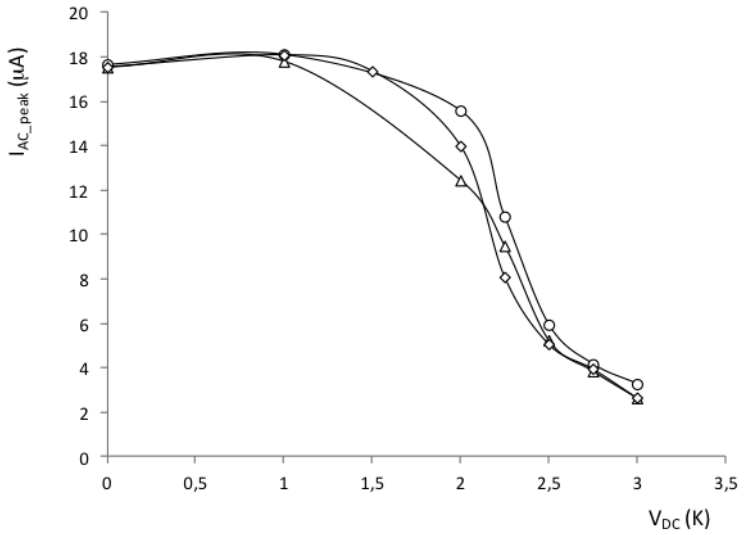

Figure A.1.: This figure shows the voltage drop for a sample with a electrode diameter of 48 mm, $\lambda = 4{,}4$ and for the frequencies 10 Hz, 100 Hz and 1000 Hz.

A.1.2. Conclusion

After $2,0\,kV$ the current drops dramatically and after $3,0\,kV$ we only measure EMC after $3,0\,kV$ it was not possible to measure the peak current. Therefore, the maximum DC voltage for measuring the capacitance is limited to $2,0\,kV$.

A.2. Capacity calculation (Excel)

Channel A (mV): when the voltage (mV) is divided by the resistance (1 kOhm) the current flowing through the curcuit, is expressed in µA.

Channel B (mv): measures the source voltage and the unit of the source voltage is V, due to the high voltage probe (x1000)

Sample	Time	Current	Voltage
	(ms)	(µA)	(V)
1	-0.86	3.48	-9.13
2	-0.83	3.49	-8.88
3	-0.81	3.50	-8.64
4	-0.78	3.51	-8.45
5	-0.76	3.52	-8.21
6	-0.73	3.53	-7.97
7	-0.71	3.54	-7.75
8	-0.68	3.55	-7.54
9	-0.66	3.56	-7.29
10	-0.64	3.57	-7.08
998	23.50	6.39	148.36
999	23.52	6.38	148.39
1000	23.55	6.38	148.43
1001	23.57	6.37	148.43
1002	23.59	6.37	148.46
1003	23.62	6.36	148.46
1695	40.54	0.21	84.06
1696	40.56	0.20	83.84
1697	40.59	0.19	83.66
1698	40.61	0.18	83.48
1699	40.64	0.17	83.26
1700	40.66	0.16	83.08

Voltage approximation

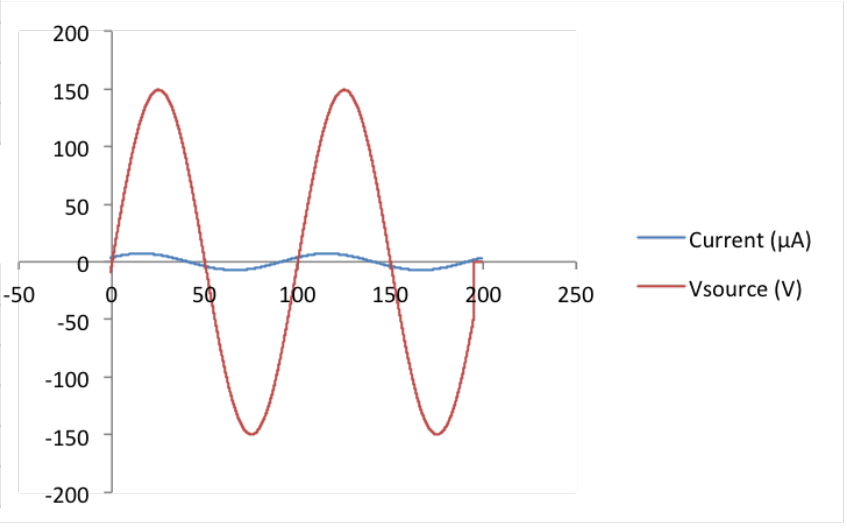

The voltage is recalculated for each cell by:
V (s) = I(s) x Zr + I(s-1000) x Zc
And s is the number of the sample in the sequence, it starts wit sample 1000 and ends with sample 8000. So 1/4 of a period is lost.

Zc = 1
Zr = 1

Sample	Time	Current	Voltage	Calculated B	error
	(ms)	(µA)	(V)	(mV)	(mV)
1000	23.55	6.38	148.43	146.03	2.40
1001	23.57	6.37	148.43	146.02	2.40
1002	23.59	6.37	148.46	146.04	2.41
1003	23.62	6.36	148.46	146.05	2.40

1000	23.64	6.36	148.49	6.96	141.52
1001	23.67	6.35	148.52	6.99	141.53
1002	23.69	6.35	148.52	7.00	141.52
1003	23.72	6.34	148.55	7.02	141.52
1004	23.74	6.34	148.55	7.04	141.51
1005	23.77	6.33	148.58	7.06	141.52
1006	23.79	6.33	148.61	7.08	141.53
1007	23.81	6.32	148.61	7.10	141.51
1008	23.84	6.32	148.64	7.12	141.52
1009	23.86	6.31	148.64	7.14	141.50
1010	23.89	6.30	148.67	7.15	141.52
1011	23.91	6.30	148.67	7.17	141.50

Voltage approximation

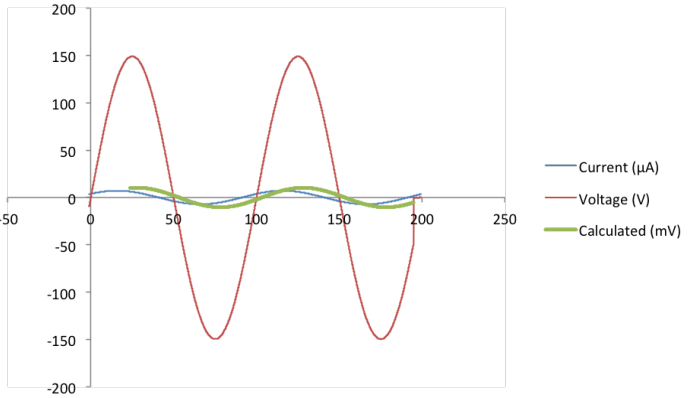

The error in between the actual voltage and the calculated voltage (absolute value)

Sample	Time	Current	Voltage	Calculated B	error
	(ms)	(μA)	(V)	(mV)	(mV)

avg (error) = 0.48

498	11.20	6.87	95.81	/	/
499	11.22	6.87	95.99	/	/
500	11.25	6.88	96.14	/	/
501	11.27	6.88	96.33	/	/
502	11.30	6.88	96.51	/	/

The value of the impedances can be found by a set of 2 equations:
V(1500) = I(1500) x Zr + I(500) x Zc
V(3500) = I(3500) x Zr + I(2500) x Zc
Solution:
Zc = 17.67 and Zr = 11.10

The value of the impedances is MOhm, due to the fact that the current expressed in μA (10^{-6}) and the voltage in V.

To further reduce the error an average is made, so by itterating the values of Zc and Zr the error can be reduced significantly.

1498	35.62	2.31	117.48	117.53	0.06
1499	35.65	2.30	117.32	117.40	0.07
1500	35.67	2.29	117.23	117.24	0.01
1501	35.70	2.28	117.11	117.12	0.01
1502	35.72	2.27	116.96	116.95	0.01
1503	35.75	2.26	116.84	116.82	0.02

2497	60.15	-6.60	-88.39	-90.57	2.18
2498	60.17	-6.60	-88.57	-90.77	2.19
2499	60.20	-6.60	-88.76	-90.92	2.17
2500	60.22	-6.61	-88.97	-91.12	2.15
2501	60.24	-6.61	-89.15	-91.32	2.17
2502	60.27	-6.62	-89.31	-91.50	2.19
2503	60.29	-6.62	-89.49	-91.68	2.19

3498	84.62	-2.84	-123.70	-123.96	0.26
3499	84.65	-2.83	-123.58	-123.81	0.23
3500	84.67	-2.82	-123.46	-123.70	0.24
3501	84.69	-2.82	-123.34	-123.61	0.28
3502	84.72	-2.80	-123.18	-123.46	0.28
3503	84.74	-2.80	-123.06	-123.35	0.29

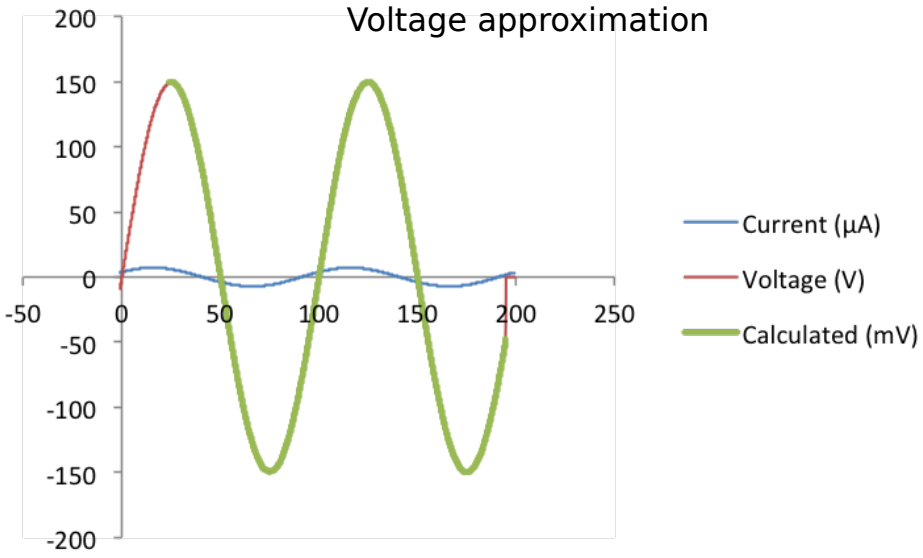

A.3. 3M VHB Tapes Technical Data

Additional Typical Performance Characteristics

Note: The following technical information and data should be considered representative or typical only and should not be used for specification purposes.

Outgassing:

3M™ VHB™ Tapes	% TML	%VCM	%WVR
4930	0.77	0.01	0.21
4932	2.41	0.66	0.23
4945	1.24	0.01	0.19

TML - Total Mass Loss

VCM - Volatile Condensible Materials

WVR - Water Vapor Regained

NASA Reference Publication, "Outgassing Data for Selecting Spacecraft Materials", (11/18/2004) Available online at http://outgassing.nasa.gov

Dielectric Constant
(ASTM D150)

3M™ VHB™ Tapes	Dielectric Constant	Dissipation Factor
4941 at 1 kHz	2.29	0.0245
at 1 MHz	1.99	0.0374
5952 at 1 kHz	2.14	0.0065
at 1 MHz	1.95	0.0506
4950 at 1 kHz	2.28	0.0227
at 1 MHz	1.99	0.0370
4910 at 1 kHz	3.21	0.0214
at 1 MHz	2.68	0.0595
4611 at 1 kHz	2.80	0.0130
at 1 MHz	2.43	0.0564

Dielectric Breakdown Strength
(ASTM D149)

3M™ VHB™ Tapes	(in volts/mil)
4941	360
4926	330
5952	455
5925	520
4950	460
4920	640
4910	630
4611	330

Thermal Conductivity - K-value

3M™ VHB™ Tapes	BTU in/ hr ft² °F	(w/mK)
4941	0.53	(0.08)
5952	0.37	(0.05)
4950/4945	0.63	(0.09)
4910	1.09	(0.16)
4611	0.77	(0.11)

$$R\text{-Value} = \frac{\text{thickness}}{\text{K-value}}$$

(When units of K-value are BTU-in/hr ft² °F and thickness is given in inches.)

Resistivity
(ASTM D257)

3M™ VHB™ Tapes	Volume Resistivity (in ohm-cm)	Surface Resistance (in ohms/square)
4914	1.7×10^{11}	$>10^{16}$
4941	2.1×10^{14}	2.7×10^{14}
5952	2.5×10^{14}	$>10^{16}$
4950	1.5×10^{15}	$>10^{16}$
4920	1.7×10^{15}	$>10^{16}$
4910	3.1×10^{15}	$>10^{16}$
4611	1.4×10^{15}	$>10^{16}$

Water Vapor Transmission Rate (WVTR)
(ASTM F1249) at 38°C/100% RH

3M™ VHB™ Tapes	
4950	14.0 g/(m² day)
4941	25.6 g/(m² day)
5952	37.1 g/(m² day)

Typical 3M™ VHB™ Tape Properties for Modeling

Thermal Coefficient of Expansion
1×10^{-4} in/in/°F
1.8×10^{-4} mm/mm/°C

Shear Modulus (@25°C, 1 Hz)
4950 Family: 6×10^{5} Pa
4941 Family: 3×10^{5} Pa

(Shear Modulus is both temperature and frequency dependent).

Youngs Modulus: For VHB tapes the Youngs Modulus will be about 3 times the Shear Modulus.

Poisson's Ratio
0.49

Burn Characteristics 3M™ VHB™ Tape 5958FR

Meets FAR 25.853 (a) 12 second vertical burn, Appendix F, Part I (a)(ii).

Meets NBS Smoking Density (ASTM F814/E662).

Meets Toxicity (Draeger Tube ABD0031, AITM 3.0005)

3M™ VHB™ Tapes
UL746C Listings - File MH 17478

Category QOQW2 Component - Polymeric Adhesive Systems, Electrical Equipment

3M™ VHB™ Tapes/ Product Families	Substrates	Temperature Rating Minimum	Maximum
4919F, 4926, 4936, 4936F, 4941, 4941F, 4947F, 4956, 4956F, 4979F	Ceramic	-35°C	110°C
	Aluminum, Galvanized steel, stainless steel, enameled steel, nickel coated ABS, glass (with or without silane coating) PVC, glass/epoxy, PBT, polycarbonate, acrylic/polyurethane paint, polyester paint	-35°C	90°C
	ABS	-35°C	75°C
4914, 4920, 4930, 4950	Aluminum, galvanized steel, enameled steel, stainless steel, ceramic, glass/epoxy	-35°C	110°C
	PBT, Acrylic	-35°C	90°C
	ABS, Polycarbonate, Rigid PVC	-35°C	75°C
4945, 4946	Phenolic, aluminum, galvanized steel, alkyd enamel	-35°C	110°C
	ABS, polycarbonate, polyimide, stainless steel, acrylic/polyurethane paint, polyester paint	-35°C	90°C
	unplasticized PVC	-35°C	75°C
5915, 5915P, 5925, 5925P, 5930, 5930P, 5952, 5952P 5962, 5962P	Polycarbonate, Primer 94 coated polycarbonate, aluminum, acrylic/ polyurethane paint, galvanized steel, steel, polyester paint, epoxy/polyester paint, epoxy paint, glass (with or without silane coating), stainless steel, enameled steel, glass epoxy, polybutylene terephthalate, Nylon®, Noryl® (PPE) polyphenenlene ether	-35°C	90°C
	Rigid PVC, ABS	-35°C	75°C
5915, 5925, 5930, 5952	Acrylic	-35°C	90°C
5962	Acrylic	-35°C	80°C
5952	Cellulose Acetate Butyrate	-35°C	90°C
4991	Polycarbonate, aluminum, acrylic/ polyurethane paint, polyester paint	-35°C	90°C
4611, 4646, 4655	Stainless steel, aluminum, galvanized steel, glass, glass/epoxy, phenolic	-35°C	110°C
	Nylon, polycarbonate	-35°C	90°C
	ABS, rigid PVC	-35°C	75°C
4905, 4910	Polycarbonate, aluminum, acrylic/polyurethane paint	-35°C	90°C

A current list can be found at www.ul.com (select certifications, search file MH17478)

Solvent and Fuel Resistance

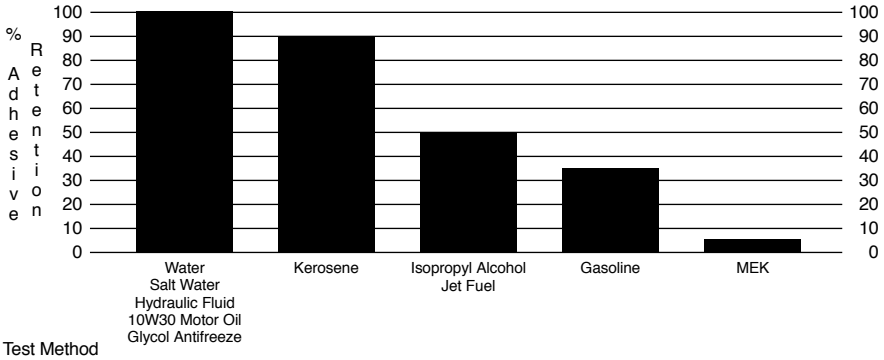

Test Method
- Tape between stainless steel and aluminum foil.
- 72 hours dwell at room temperature.
- Solvent immersion for 72 hours.
- Test within 45 minutes after removing from solvent.
- 90° peel angle.
- 12 in./min. rate of peel.
- Peel adhesion compared to control.

Note: Continuous submersion in chemical solutions is not recommended. The above information is presented to show that occasional chemical contact should not be detrimental to tape performance in most applications in ordinary use.

A.4. Drawings scissors mechanism

004	1	plexiglass (plate)	700 x 1000 x 4 (mm)	
003	112	Hexagon thin nut	ISO 4036 - M3	
002	56	Pan head screw (cross)	ISO 7045 - M3 x 14 - 4,8 - H	
001	168	Plain washer	ISO 7091 - ST 3 - 100 HV	nylon
Number	Amount	Name	Norm	Notes

Materials

Student1:	Name : Dimitri Lethion	Date: 24/04/2014
Student2:	Name : Raphaël Vorias	

	Title: scissors mechanism	**Dev Nr.: 01**

Sub Assembly A

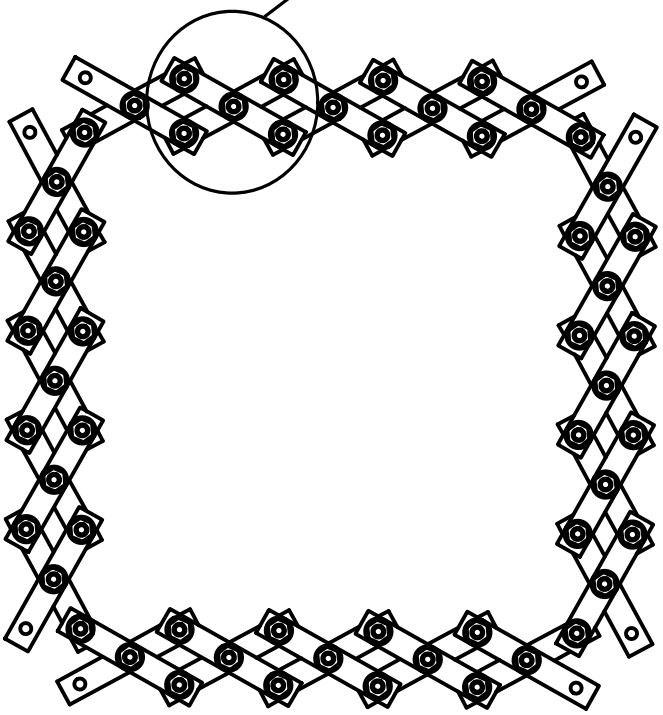

Assembly A

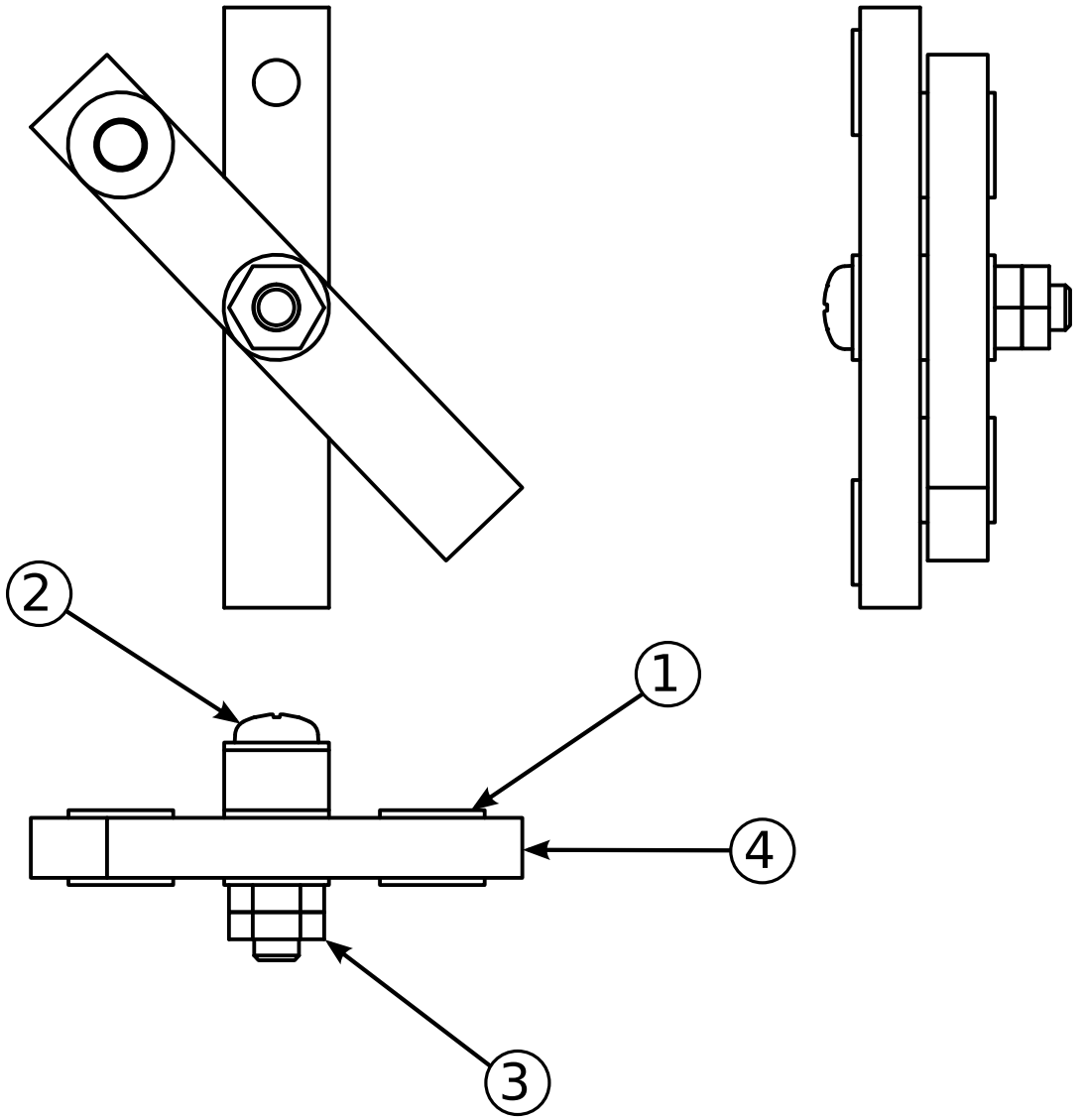

Sub Assembly A

PRODUCED BY AN AUTODESK EDUCATIONAL PRODUCT
PRODUCED BY AN AUTODESK EDUCATIONAL PRODUCT
PRODUCED BY AN AUTODESK EDUCATIONAL PRODUCT

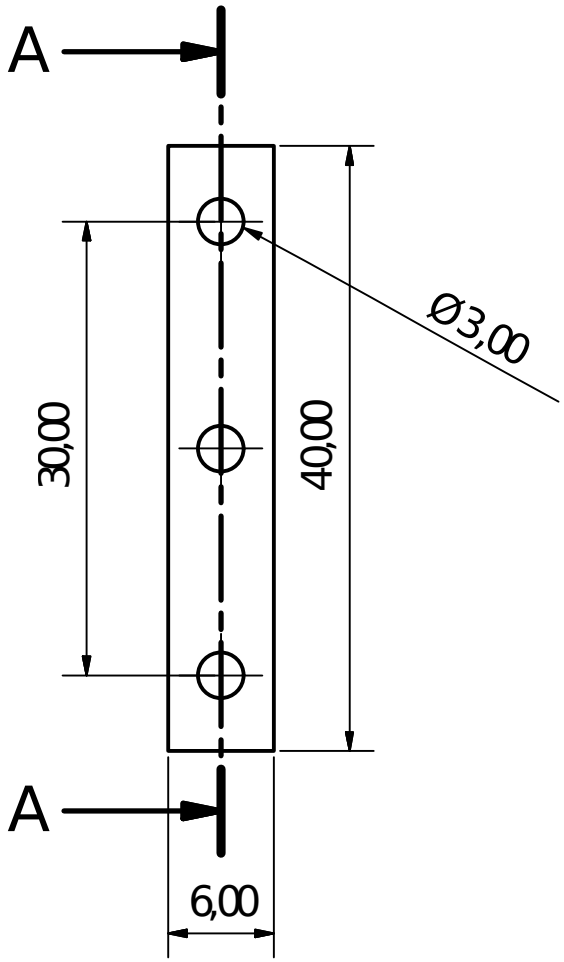

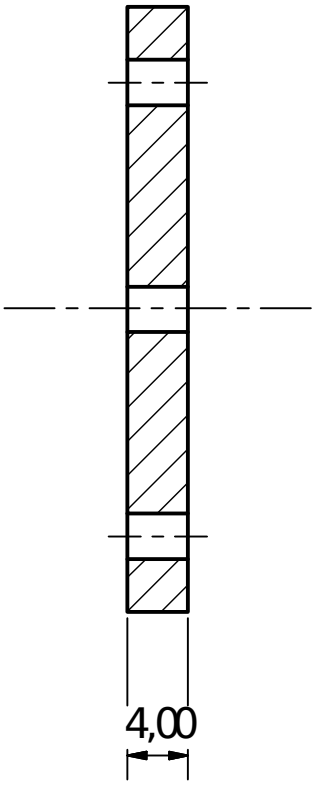

Drawing 1

A.5. OFV 5000 vibrometer controller

Polytec

OFV-5000 Vibrometer Controller

Modular Vibrometer System

- **OFV-5000 Vibrometer Controller**
  Velocity Decoders
  Displacement Decoders
- OFV-505/503
  Standard Sensor Heads
- OFV-551/552
  Fiber Interferometers
- OFV-534
  Compact Sensor Head

Measuring Vibrations

Polytec's modular vibrometer controller is continually improving to meet the needs of advanced vibration measurement applications. The latest design adds digital processing with a range of new features that make non-contact vibration analysis even more precise, simple, flexible and rewarding.

OFV-5000 Controller – The Soul of a Quality Vibrometer System

The OFV-5000 Vibrometer Controller features excellent vibration resolution and dynamic range from a choice of digital/analog decoders, remote focus and focus memory (with OFV-505), high capacity for a wide range of modules and filtering. Polytec Laser Doppler Vibrometers operate on the Doppler principle, measuring back-scattered laser light from a vibrating structure, to determine its vibrational velocity and displacement.

A vibrometer system is comprised of controller electronics and a non-contact standard-optic or fiber-optic sensor head. The controller provides signals and power for the sensor head, and processes the vibration signals. These are electronically converted by specially developed decoders within the controller to obtain velocity and displacement information about the test structure. This information is provided by OFV-5000 in either analog or digital form, for further data evaluation.

Functionality and Flexibility

- **Modular Approach**
  A wide range of configurations offers optimum performance for the task with maximum flexibility and expandability to meet future needs.
- **Application-Specific Configuration**
  By selecting from a choice of different analog and/or digital decoders, performance can be precisely tailored to match the demands of the application. Several compatible standard-optic and fiber-optic sensor heads are available to meet specific needs for robustness, flexibility and ease-of-use.
- **Upgradeable to Scanning Vibrometer**
  OFV-5000 is fully upgradeable to Polytec's 1-D and 3-D Scanning Vibrometer systems for full field vibration analysis.
- **Remote Focus Functions**
  Autofocus, remote focus and focus memory are all possible with the OFV-5000 controller used with the OFV-505 sensor head.

Laser Vibrometry Expansion Options, using the OFV-5000 Controller

Flexible Signal Processing

The OFV-5000 controller is designed to accept a choice of signal processing modules, each optimized for different frequency, velocity or displacement performance.

Each module is therefore tuned for different measurement tasks by making the best use of the vibration information in the Doppler signal obtained by the sensor head.

Various analog and/or digital decoder options seamlessly cover the entire velocity range up to ±10 m/s, displacements from the picometer to the meter range, and frequencies from DC to 24 MHz. Up to four decoders can be installed simultaneously to obtain the greatest possible flexibility. This flexibility also allows add-ons and modifications to meet future needs.

Vibrometer Measurement System

A system comprises an OFV-5000 controller, a choice of decoder modules and a sensor head. A choice of compact or standard single-point and fiber-delivered sensors, or dual (differential) fiber sensors is available.

Expansion to Scanning Vibrometer Systems

A system based on the OFV-5000 can be extended to a full scanning vibrometer system by adding other components.

The PSV-400 Scanning Vibrometer makes it possible to rapidly and automatically acquire vibration characteristics of complete surfaces, while the PSV-400-3D extends this to three-dimensional data acquisition and analysis. The MSV-400 Micro Scanning Vibrometer and MSA-500 Micro System Analyzer have been developed to perform the same measurements on microstructures.

Selection and Combination of Signal Decoders

The OFV-5000 controller has four internal slots to accept up to four different signal decoders, depending on the desired measurement ranges. Two are specifically designated for velocity decoders and one is for the displacement decoder. An Auxiliary Slot is provided to take a further optional velocity or displacement decoder.

Please contact your local vibrometer sales or application engineer who will help you to select the appropriate decoders and VibSoft data acquisition packages.

Velocity Decoders

Velocity decoders are designed to acquire vibrations in a wide range of frequencies from 0 up to 24 MHz, meeting the specific needs of your application. Besides the general purpose decoders VD-02, VD-04, VD-09 and VD-06, special purpose decoders for high frequencies (VD-05, 10 MHz) are available. Combining these decoders extends the available ranges or adds additional resolution to the OFV-5000 controller system.

Please refer to the "Table of Decoder Combinations" for possible combinations and to the Technical Data section for details about the decoders.

Displacement Decoders

The analog DD-100 and DD-200 14 bit displacement decoders take phase information from the Doppler signal to provide direct displacement signals, not derived from the velocity information. They may be used in conjunction with velocity decoders to provide full vibration characterization of the test structure.

Alternatively, OFV-5000 accepts the DD-500 digital displacement decoder with high resolution digital/analog output, or the DD-900 which is a high resolution and high frequency digital displacement decoder.

A further option is the DD-600 I&Q demodulator. This is designed to allow processing of the digital signal with the PC-based VibSoft-VDD package. This provides the highest resolution and dynamic range of all the displacement decoder options.

DD-300 and DD-400 decoders are designed for use in the Auxiliary Slot. The high frequency DD-300 measures between 50 kHz and 24 MHz. The DD-400 employs an analog integrator for the frequency range up to 250 kHz.

DSP Filter

The DSP based adaptive filter module significantly improves the signal-to-noise ratio of the vibration signal by suppressing random and non-periodic noise for frequencies ranging from DC to 20 kHz. The adaptive filter can only be used in conjunction with the digital decoder VD-06.

Table of Decoder Combinations

Main Velocity Decoder		Main Displacement Decoder		Auxiliary Decoder		DSP Filter	S/P-DIF
Slot 1	Slot 2	14-bit or FC	16-bit DSP	Velocity or Displacement			
VD-02	–	DD-100 or DD-200	–	VD-05	DD-300	n.a.	no
VD-02	VD-06		DD-500			LF-02	yes
VD-04	–		–		DD-400 or DD-300	n.a.	no
VD-04	VD-06		DD-500			LF-02	yes
–	VD-06		DD-500		DD-300	LF-02	yes
VD-09	–	n.a.	DD-900			n.a.	no
VD-09	VD-06	n.a.	DD-900			LF-02	yes

Instead of the internal displacement decoder, a DD-600 I&Q demodulator for external PC-based signal processing can also be installed (VibSoft-VDD)

OFV-5000 Technical Data

General Specifications	
Operating temperature	+ 5 °C … +40 °C (41 °F ... 104 °F)
Storage temperature	–15 °C ... +65 °C (5 °F ... 149 °F)
Relative humidity	Max. 80 %, non-condensing
Power supply	100...240 VAC ±10 %, 50/60 Hz, max. 100 VA
Weight	10 kg
Dimensions [W x H x L]	450 mm x 360 mm x 150 mm (19" rack mount)
Interface	RS-232
Display	Illuminated graphics LCD with menu assistance
Outputs analog	On the front: Velocity out, Displacement out, DSP out, Auxiliary out; On the back: Signal level out
Outputs digital	S/P-DIF optical and electrical

Sensor Head Compatibility	
Standard single point sensor heads	OFV-505, OFV-503, OFV-534
Fiber optic sensor heads	OFV-551, OFV-552

Available Velocity Decoders	
Analog decoders	
VD-02	max. 1.5 MHz, 4 measurement ranges (mm/s/V): 5, 25, 125, 1000
VD-04	max. 250 kHz, 3 measurement ranges (mm/s/V): 10, 100, 1000
VD-05	max. 10 MHz, 2 measurement ranges (mm/s/V): 100, 500
Digital decoders	
VD-06	max. 350 kHz, 4 measurement ranges (mm/s/V): 1, 2, 10, 50
VD-09	max. 2.5 MHz, 14 measurement ranges (mm/s/V): 5 ... 1,000

Available Displacement Decoders	
DD-100	14 bit FC decoder, 250 kHz, 8 measurement ranges
DD-200	14 bit FC decoder, 250 kHz, 13 measurement ranges
DD-300	Ultrasonic displacement decoder, 24 MHz, 1 measurement range
DD-400	Analog integrator, 250 kHz, 3 measurement ranges
DD-500	16 bit DSP decoder, 350 kHz, 16 measurement ranges
DD-900	Broadband digital displacement decoder, 2.5 MHz, 16 measurement ranges
DD-600	I&Q decoder, direct output of the quadrature signal, optional further processing with VibSoft-VDD

Adaptive Filter Module	
LF-02	DSP based, analog and digital output signal, frequency range: 0 … 20 kHz

For more information on signal decoders please see the "Decoder Guidelines" data sheet and the respective decoder data sheets, or contact your local sales/application engineer. The data sheets can be downloaded from **www.polytec.com/vibrometers**

Polytec GmbH (Germany)
Polytec-Platz 1-7
76337 Waldbronn
Tel. +49 7243 604-0
Fax +49 7243 69944
info@polytec.de

Polytec France S.A.S.
Bâtiment Orion – 1er étage
39, rue Louveau
92320 Châtillon
Tel. +33 1 496569-00
Fax +33 1 57214068
info@polytec.fr

Polytec Ltd.
(Great Britain)
Lambda House, Batford Mill
Harpenden, Herts AL5 5BZ
Tel. +44 1582 711670
Fax +44 1582 712084
info@polytec-ltd.co.uk

Polytec Japan
Arena Tower, 13th floor
3-1-9, Shinyokohama,
Kohoku-ku, Yokohama-shi,
Kanagawa, 222-0033
Tel. +81 45 478-6980
Fax +81 45 478-6981
info@polytec.co.jp

Polytec, Inc. (USA)
North American Headquarters
16400 Bake Parkway
Suites 150 & 200
Irvine, CA 92618
Tel. +1 949 943-3033
Fax +1 949 679-0463
info@polytec.com

Central Office
1046 Baker Road
Dexter, MI 48130
Tel. +1 734 253-9428
Fax +1 734 424-9304

East Coast Office
25 South Street, Suite A
Hopkinton, MA 01748
Tel. +1 508 417-1040
Fax +1 508 544-1225

www.polytec.com

A.6. Picoscope 4000 series (4424)

pico® Technology

PicoScope® 4000 Series

HIGH-PRECISION USB OSCILLOSCOPES

For detailed waveforms and accurate measurements

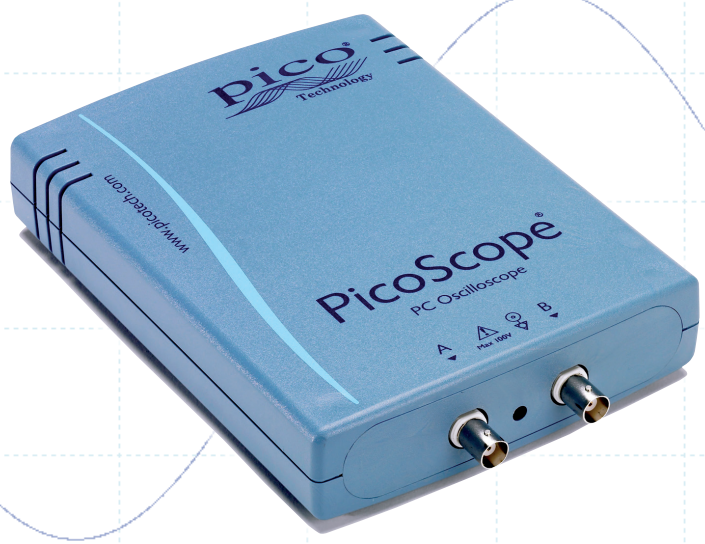

- 32 MS buffer
- 12 bit resolution
- 80 MS/s sampling
- 20 MHz bandwidth
- 2 or 4 channels
- 2 channel IEPE model
- USB powered

32 MS BUFFER

12 BITS

IEPE

5 YEAR WARRANTY

- Free technical support • Free upgrades
- Supplied with SDK including example programs
- Software compatible with Windows XP, Vista, 7 and 8

www.picotech.com

PicoScope features at a glance

- 20 MHz oscilloscope and FFT spectrum analyzer
- 26 automatic measurements
- Mask limit testing with alarms
- Serial bus decoding
- Per-channel low-pass filtering
- Software resolution enhancement to 16 bits
- Math channels with basic and advanced functions
- Reference waveforms
- Waveform buffer with up to 10,000 segments and overview window
- Digital color and analog intensity persistence display modes
- XY mode

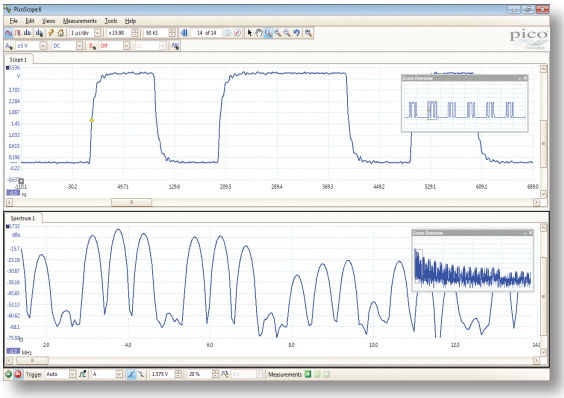

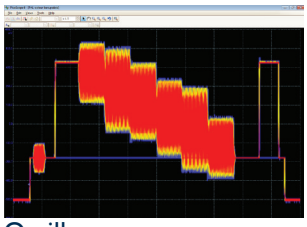

Oscilloscope

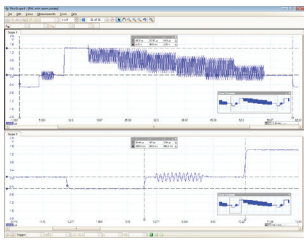

Quick and powerful zoom

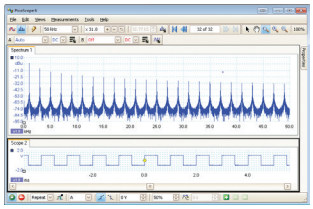

Spectrum analyzer

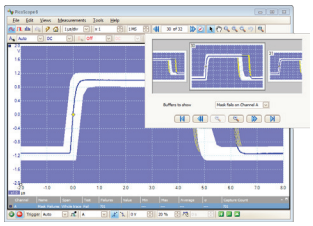

Mask limit testing

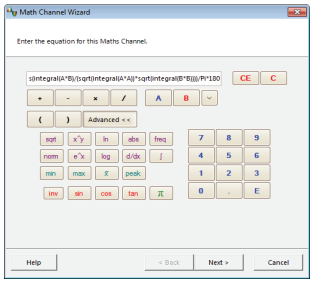

Math channels

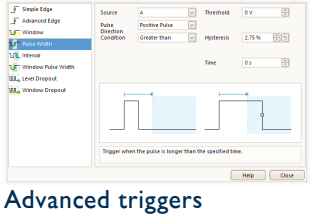

Advanced triggers

All-in-one instruments

The PicoScope 4000 Series PC Oscilloscopes are extremely versatile, with an oscilloscope and spectrum analyzer included in every model.

PicoScope 4224 IEPE

The 2-channel IEPE version is compatible with industry-standard IEPE (integrated electronics piezoelectric) accelerometers and microphones, making it suitable for a variety of measurement applications including noise and vibration analysis.

Convenience and speed

The PicoScope 4000 Series scopes obtain their power from the USB 2.0 interface, so there's no need for an external power supply. The USB port also delivers high-speed data to your PC to give you a responsive, high-resolution display. A maximum sampling rate of 80 MS/s is combined with a high resolution of 12 bits, giving you 16 times better vertical resolution than most standard scopes.

Deep memory

The 32 M sample buffer is 'always on'. There is never a compromise between buffer size and waveform update rate, because the PicoScope 4000 Series always maximises both at the same time. Now you can capture every waveform with full detail without having to think about it.

Advanced software

The scopes are bundled with the latest version of PicoScope for Windows. PicoScope is easy to use and can export data in a variety of graphical, text and binary formats. Also included are Windows drivers and example programs.

Mask limit testing

PicoScope allows you to draw a mask around any signal with user-defined tolerances. This has been designed specifically for production and debugging environments, enabling you to compare signals. Simply capture a known good signal, draw a mask around it, and then attach the system under test. PicoScope will capture any intermittent glitches and can show a failure count and other statistics in the Measurements window.

The numerical and graphical mask editors can be used separately or in combination, allowing you to enter accurate mask specifications, modify existing masks, and import and export masks as files.

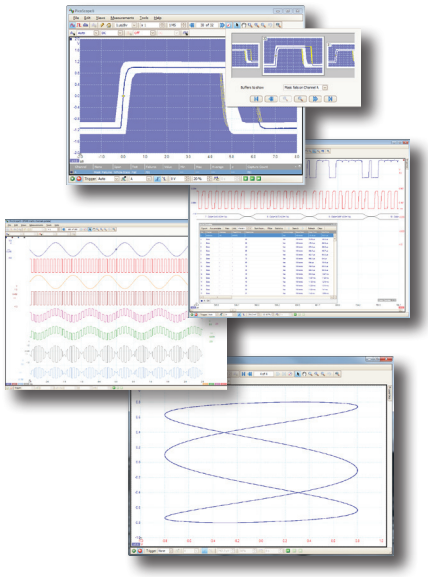

Math channels

With PicoScope you can perform a variety of mathematical calculations on your input signals and reference waveforms.

Use the built-in list for simple functions such as addition and inversion, or open the equation editor and create complex functions involving trigonometry, exponentials, logarithms, statistics, integrals and derivatives.

Advanced triggers

As well as the standard range of triggers found on most oscilloscopes, the PicoScope 4000 Series offers one of the best selections of advanced triggers available. These include pulse width, windowed and dropout triggers to help you find and capture your signal quickly.

MODEL SELECTOR

MODEL	BANDWIDTH	CHANNELS	SAMPLING	BUFFER MEMORY	EXT TRIG	AWG
PicoScope 4424	20 MHz	4	80 MS/s	32 MS	No	No
PicoScope 4224	20 MHz	2	80 MS/s	32 MS	No	No
PicoScope 4224 IEPE	20 MHz	2	80 MS/s	32 MS	No	No

SPECIFICATIONS

MODEL	PicoScope 4424	PicoScope 4224	PicoScope 4224 IEPE	
			Passive Probe Mode	IEPE Interface Mode
INPUTS				
Number of channels	4 BNC inputs	2 BNC inputs	2 BNC inputs	
Analog bandwidth	DC to 20 MHz (10 MHz on ±50 mV range)		DC to 20 MHz	1.6 Hz to 20 MHz
Rise time (10% to 90%, calculated)	17.5 ns (35 ns on ±50 mV range)			
Voltage ranges	±50 mV to ±100 V in 11 ranges		±50 mV to ±20 V in 9 ranges	
Sensitivity	10 mV/div to 20 V/div		10 mV/div to 4 V/div	
Graphing frequency measurement	20 Hz, 200 Hz, 2 kHz, and 20 kHz ranges			
Vertical resolution	12 bits (up to 16 bits with resolution enhancement)			
Input coupling	AC or DC, software-controlled			
Input impedance	1 MΩ ‖ 22 pF		1 MΩ ‖ 22 pF	1 MΩ ‖ 1 nF
Overvoltage protection	±200 V		±100 V	
SAMPLING				
Timebases	100 ns/div to 5000 s/div			
Maximum sampling rate (real time)	1/2 channels: 80 MS/s* 3/4 channels: 20 MS/s	80 MS/s	80 MS/s	
	* To achieve the stated sampling rate with two channels, choose one channel from A or B and one from C or D.			
Buffer size	32 MS shared between active channels			
TRIGGERING				
Sources	Any input channel			
Modes	None, single, repeat, auto, rapid			
Trigger types	Rising edge, falling edge, edge with hysteresis, pulse width, runt pulse, dropout, windowed			
PERFORMANCE				
Timebase accuracy	50 ppm			
DC accuracy	1% of full scale			
Trigger resolution	1 LSB			
Trigger re-arm time	2.5 µs (fastest timebase)			
ENVIRONMENT				
Temperature range	Operating: 0 °C to 45 °C For stated accuracy: 20 °C to 30 °C Storage: –20 °C to 60 °C			
Humidity range	Operating: 5% to 80% RH, non-condensing Storage: 5% to 95% RH, non-condensing			
PC connection	USB 2.0. Compatible with USB 1.1 and USB 3.0.			
PC operating system	Windows XP (SP3), Windows Vista, Windows 7 and Windows 8 (not Windows RT) 32-bit and 64-bit versions			
Power supply	Powered by USB port			
Dimensions	200 mm x 140 mm x 38 mm including connectors			
Weight	< 500 g			
Compliance	EU EMC and LVD Standards RoHS and WEEE, FCC Rules Part 15 Class A			

PicoScope 4000 Series

What do I get?

The PicoScope 4000 Series oscilloscope are available individually, or in kits containing the following items.

- PicoScope 4000 Series PC oscilloscope
- Passive x1/x10 60 MHz probes (2 or 4)
- Quick start guide
- USB 2.0 cable
- PicoScope software CD
- Tough, padded carrying case

Also available in the PicoScope 4000 Series

PicoScope 4262

- 16-bit resolution
- Low noise and distortion
- Arbitrary waveform generator
- 16 MS buffer
- 10 MS/s sampling rate
- 5 MHz bandwidth

PicoScope 4824

- 8 input channels
- 256 MS buffer
- SuperSpeed USB 3.0 interface
- Arbitrary waveform generator
- 12-bit resolution
- 80 MS/s sampling rate

PicoScope 2000 Series
Ultra-compact and handheld

PicoScope 3000 Series
General-purpose 2 and 4 channel

PicoScope 5000 Series
Flexible resolution 8 to 16 bits

PicoScope 6000 Series
High performance Up to 1 GHz

PicoScope 9000 Series
20 GHz sampling with TDR/TDT

For more information on any of these products, visit www.picotech.com.

Ordering information

ORDER CODE	PART DESCRIPTION	GBP*	USD*	EUR*
PP493	PicoScope 4424 oscilloscope	799	1319	967
PP479	PicoScope 4424 oscilloscope kit, with 4 probes	825	1362	999
PP492	PicoScope 4224 oscilloscope	499	824	604
PP478	PicoScope 4224 oscilloscope kit, with 2 probes	519	857	628
PP695	PicoScope 4224 IEPE oscilloscope	599	989	725

* Prices exclude VAT and are correct at the time of publication.
Please contact Pico Technology for the latest prices before ordering.

UK headquarters:
Pico Technology
James House
Colmworth Business Park
St. Neots
Cambridgeshire
PE19 8YP
United Kingdom
☎ **+44 (0) 1480 396 395**
🖷 **+44 (0) 1480 396 296**
✉ **sales@picotech.com**

USA headquarters:
Pico Technology
320 N Glenwood Blvd
Tyler
Texas 75702
United States
☎ **+1 800 591 2796**
🖷 **+1 620 272 0981**
✉ **sales@picotech.com**

www.picotech.com

A.7. Tektronix P6015 A high voltage probe

Passive High Voltage Probes

P5100A-TPP0850-P5122-P5150-P6015A Datasheet

Safe high voltage probe solutions for ground-referenced voltage testing. It is critical to safely and accurately capture real-time signal information from "elevated" or "floating" voltage systems. Our portfolio of high voltage probes provides the safety you need for single-ended, differential or isolated measurements.

Key performance specifications

- P5100A
  - DC to 500 MHz
  - 2500 V_{Peak}, 1000 V_{RMS} CAT II
  - 100X with readout coding
- TPP0850
  - DC to 800 MHz
  - 2500 V_{Peak}, 1000 V_{RMS} CAT II
  - 50X with readout coding
  - Designed for use with the MSO/DPO5000 and MSO/DPO4000B Series Oscilloscopes
- P5122
  - DC to 200 MHz
  - 1000 V_{RMS} CAT II when DC-coupled*[1]
  - 100 X
  - Floatable up to 600 V_{RMS} CAT II
  - For TPS2000 and THS3000 Series Oscilloscopes
- P5150
  - DC to 500 MHz
  - 2500 V_{Peak}, 1000 V_{RMS} CAT II
  - 50 X
  - Floatable up to 600 V_{RMS} CAT II or 300 V_{RMS} CAT III
  - For TPS2000 and THS3000 Series Oscilloscopes
- P6015A
  - DC to 75 MHz
  - High Voltage - 20 kV DC / 40 kV Peak (100 ms Pulse Width)
  - Optional 1000X readout coding

Applications

- Power supply design
- Design motor drive
- Electronic ballast
- Power semiconductors
- Switch mode control
- UPS systems
- Power converters

P5100A High-Voltage Probe

The P5100A is a low input capacitance, high-voltage probe (2.5 kV) designed for higher-frequency applications. The probe can be compensated to match plug-ins and oscilloscopes with nominal input capacitances of 7-30 pF. A variety of screw-on accessories provide easy connection to the device-under-test.

TPP0850 High-Voltage Probe

The TPP0850 offers the industry's highest bandwidth probe (800 MHz) for high-voltage signals (up to 2500 V_{p-p}). This is ideal for testing power semiconductors and switch-mode power supplies, which continue to increase in switching speed to minimize power loss, creating a need for faster rise time, higher bandwidth, and higher voltage probes. The TPP0850 meets this need and can be used with switching transistor circuits operating at 1200 V_{RMS}, above the voltage operating range of standard general-purpose probes. It will also be able to accommodate emerging power applications that will require even faster rise time capabilities.

P5150 and P5122 IsolatedChannel™ Applications

In many applications, it is important to be able to isolate the measurement from earth ground and also to isolate the common voltage between channels. The P5150 or P5122, coupled with the TPS2000 and THS3000 Series digital storage oscilloscopes, deliver both the isolation for the measurement from earth ground and full isolation between the channels. The P5150 is the recommended probe for measuring ripple on high-voltage DC supplies. The P5122 probe should not be used on the TPS2000 Series oscilloscopes for AC-coupled measurements on signals with greater than 300 V DC offset.

P6015A High-Voltage Probe

For heavy-duty high-performance measurements of voltages over 2.5 kV, the P6015A is the industry standard. You can measure DC voltages up to 20 $kV_{RMS}$and pulses up to 40 kV (peak, 100 ms duration). The 75 MHz bandwidth enables you to capture fast, high-voltage signals.

The P6015A uses an environmentally safe silicone compound for a dielectric and never needs refilling. Other features include: A 7-49 pF compensation range, small compensation box that fits on adjacent amplifier inputs, and a readout option for use with most Tektronix digital scopes. With the readout option, displayed voltage amplitude values will be the actual signal value rather than understated by a factor of 1,000.

Note: Using the readout version with other than Tektronix digital oscilloscopes may result in an erroneous readout display.

Specifications

All specifications apply to all models unless noted otherwise.

Model overview

	P5100A	TPP0850	P5122	P5150	P6015A	P6015A Opt. 1R
Nominal length	2 m	1.3 m	1.2 m	2 m	3 m	3 m
Attenuation	100X	50X	100X	50X	1000X	1000X
Bandwidth	500 MHz	800 MHz	200 MHz	500 MHz	75 MHz	75 MHz
Rise time (typ)	<700 ps	<525 ps	2.2 ns	<700 ps	4.0 ns	4.0 ns
Loading	40 MΩ/ 2.5 pF	40 MΩ/ 1.8 pF	100 MΩ/ 4.0 pF	40 MΩ/ 3.8 pF	100 MΩ/ 3.0 pF	100 MΩ/ 3.0 pF
Maximum input voltage, DC or RMS	2.5 kV_{Peak} 1000 V_{RMS} CAT II	2.5 kV_{Peak} 1000 V_{RMS} CAT II	1000 V_{RMS} CAT II	2.5 kV_{Peak} 1000 V_{RMS} CAT II	20 kV	20 kV
Maximum float voltage	N/A	N/A	600 V_{RMS} CAT II	600 V_{RMS} CAT II 300 V_{RMS} CAT III	N/A	N/A
Compensation range (pf)	7 to 30	N/A	10 to 22	10 to 25	7 to 49	7 to 49
Readout	Yes	Yes	No	No	No	Yes

EMC environment and safety

P5100A	UL61010-031, EN61010-031, IEC61010-031, CSA61010-031
TPP0850	UL61010-031, EN61010-031, IEC61010-031, CSA61010-031
P5122	UL61010-1, UL61010B-2-031, CSA61010-1
P5150	UL61010-031, EN61010-031, IEC61010-031, CSA61010-031
P6015A	UL3111-1, EN61010-1, IEC61010-2-031, CSA1010.1, CSA1010.2.031

Ordering information

Models

P5100A/TPP0850	High Voltage Probes Includes: Large hook tip (013-0384-xx), small hook tip (013-0388-xx), 6 in. ground lead (196-3524-xx), 18 in. ground lead (196-3525-xx), ground spring (214-5298-xx), crocodile clip (344-0461-xx), adjustment tool (003-1433-xx), color bands (016-1886-xx).
P5122	100X, High-voltage Probe for TPS2000 and THS3000 Series Oscilloscopes. Includes accessory kit (020-3046-xx) Contents: large retractable hook tip, lead with hook tip, lead with crocodile clip, adjustment tool, instruction manual.
P5150	50X, High-voltage Probe for TPS2000 and THS3000 Series Oscilloscopes. Includes: Large hook tip (013-0389-xx), small hook tip (013-0388-xx), 6 in. ground lead (196-3526-xx), 18 in. ground lead (196-3527-xx), common spring (214-5299-xx), crocodile clip (344-0461-xx), color bands (016-1886-xx), adjustment tool (003-1433-xx).
P6015A	1000X, 3-meter High-voltage Probe. Includes: Hook probe tip (206-0463-xx); banana plug tip (134-0016-xx); crocodile clip - plugs onto ground lead (344-0461-xx); ground lead (196-3363-xx); carrying case (016-1147-xx); instruction manual (070-8223-xx).

Recommended accessories (for P5100A, TPP0850, P5150)

Probe Tip to BNC Adapter	013-0291-xx
0.080 in. diameter Spring Tip	206-0060-xx

Warranty

One year parts and labor.

Options

Options (P6015A only)

Option 1R	3-meter length with readout

Service options (P6015A)

Opt. C3	Calibration Service 3 Years
Opt. C5	Calibration Service 5 Years
Opt. D1	Calibration Data Report
Opt. D3	Calibration Data Report 3 Years (with Opt. C3)
Opt. D5	Calibration Data Report 5 Years (with Opt. C5)
Opt. R3	Repair Service 3 Years (including warranty)
Opt. R5	Repair Service 5 Years (including warranty)
Opt. SILV600	Standard warranty extended to 5 years

Service options (TPP0850)

Opt. C3	Calibration Service 3 Years
Opt. C5	Calibration Service 5 Years
Opt. D1	Calibration Data Report
Opt. D3	Calibration Data Report 3 Years (with Opt. C3)
Opt. D5	Calibration Data Report 5 Years (with Opt. C5)
Opt. R3	Repair Service 3 Years (including warranty)
Opt. R5	Repair Service 5 Years (including warranty)
Opt. SILV200	Standard warranty extended to 5 years

CE

Tektronix is registered to ISO 9001 and ISO 14001 by SRI Quality System Registrar.

ASEAN / Australasia (65) 6356 3900
Belgium 00800 2255 4835*
Central East Europe and the Baltics +41 52 675 3777
Finland +41 52 675 3777
Hong Kong 400 820 5835
Japan 81 (3) 6714 3010
Middle East, Asia, and North Africa +41 52 675 3777
People's Republic of China 400 820 5835
Republic of Korea 001 800 8255 2835
Spain 00800 2255 4835*
Taiwan 886 (2) 2722 9622

Austria 00800 2255 4835*
Brazil +55 (11) 3759 7627
Central Europe & Greece +41 52 675 3777
France 00800 2255 4835*
India 000 800 650 1835
Luxembourg +41 52 675 3777
The Netherlands 00800 2255 4835*
Poland +41 52 675 3777
Russia & CIS +7 (495) 6647564
Sweden 00800 2255 4835*
United Kingdom & Ireland 00800 2255 4835*

Balkans, Israel, South Africa and other ISE Countries +41 52 675 3777
Canada 1 800 833 9200
Denmark +45 80 88 1401
Germany 00800 2255 4835*
Italy 00800 2255 4835*
Mexico, Central/South America & Caribbean 52 (55) 56 04 50 90
Norway 800 16098
Portugal 80 08 12370
South Africa +41 52 675 3777
Switzerland 00800 2255 4835*
USA 1 800 833 9200

* European toll-free number. If not accessible, call: +41 52 675 3777

Updated 10 April 2013

For Further Information. Tektronix maintains a comprehensive, constantly expanding collection of application notes, technical briefs and other resources to help engineers working on the cutting edge of technology. Please visit www.tektronix.com.

01 Apr 2014

56W-10262-12

www.tektronix.com

Tektronix®

A.8. Vibrometer experimental data

λ	V [kV]	d1 [µm]	d2 [µm]	d3 [µm]	d4 [µm]	d5 [µm]	avg1 [µm]
4,4	0	0	0	0	0	0	0
	0,5	-0,64	-0,32	0	0,24	0	-0,144
	1	-1,2	-0,8	0,24	0	-0,8	-0,512
	1,5	-0,64	-0,16	0,96	-0,08	0,24	0,064
	2	0,88	1,92	2,4	1,36	1,84	1,68
	2,5	4,72	5,36	5,28	4,96	4,88	5,04
	3	11,36	7,84	8	7,36	7,36	8,384
	3,5	14,88	10,72	11,52	10,16	10,24	11,504
	4	17,68	13,68	14,32	12,88	13,28	14,368

λ	V [kV]	d1 [µm]	d2 [µm]	d3 [µm]	d4 [µm]	d5 [µm]	avg2 [µm]
4,4	0	0	0	0	0	0	0
	0,5	0,08	0	0,16	0	0,08	0,064
	1	0,24	0,32	0,72	0,48	0,56	0,464
	1,5	0,88	-0,16	1,76	1,12	1,52	1,024
	2	2,48	2,16	3,2	2,32	3,12	2,656
	2,5	3,92	3,84	4,48	3,6	4,4	4,048
	3	4,8	5,12	5,36	4,16	4,72	4,832
	3,5	5,6	6,08	6,56	4,96	5,44	5,728
	4	6,8	7,2	8	6	6,56	6,912

λ	V [kV]	d1 [µm]	d2 [µm]	d3 [µm]	d4 [µm]	d5 [µm]	avg3 [µm]
4,4	0	0	0	0	0	0	0
	0,5	-0,24	-0,08	0,08	0,4	0,16	0,064
	1	0,8	0,64	0,8	1,2	1,2	0,928
	1,5	2,88	3,2	3,04	2,88	2,64	2,928
	2	6,32	6,4	6,48	6	5,6	6,16
	2,5	12	12	9,76	10,24	9,12	10,624
	3	15,6	15,52	15,36	13,36	10,48	14,064
	3,5	17,76	18,8	18,56	16,16	13,76	17,008
	4	20,56	22,56	20,72	20,16	16,32	20,064

λ	V [kV]	d1 [µm]	d2 [µm]	d3 [µm]	d4 [µm]	d5 [µm]	avg4 [µm]
4,5	0	0	0	0	0	0	0
	0,5	0,32	0,48	0,32	0,64	0,64	0,48
	1	0,88	1,44	1,6	1,92	1,92	1,552
	1,5	2,48	3,2	3,36	3,68	3,68	3,28
	2	5,52	5,92	5,6	6,56	6,08	5,936
	2,5	9,52	9,12	8,8	10,24	9,6	9,456
	3	14,24	13,44	12,8	14,08	13,12	13,536
	3,5	18,88	20,48	17,92	19,68	19,2	19,232
	4	26,72	29,44	28,96	31,2	29,92	29,248

λ	V [kV]	d1 [µm]	d2 [µm]	d3 [µm]	d4 [µm]	d5 [µm]	avg5 [µm]
4,5	0	0	0	0	0	0	0
	0,5	0,16	-0,16	0,08	0,64	0,24	0,192
	1	0,64	0	0,72	0,64	0,64	0,528
	1,5	1,36	1,2	2,16	1,36	1,44	1,504
	2	2,88	3,52	2,88	2,4	2,48	2,832

2,5	2,88	4,96	5,36	4,56	4	4,352
3	5,12	5,76	7,84	6,4	4,96	6,016
3,5	5,84	6,24	10,16	7,12	6,88	7,248
4	7,84	8	12,96	10	10,08	9,776

V [kV]	avg_total [µm]
0	0
0,5	0,1312
1	0,592
1,5	1,76
2	3,8528
2,5	6,704
3	9,3664
3,5	12,144
4	16,0736

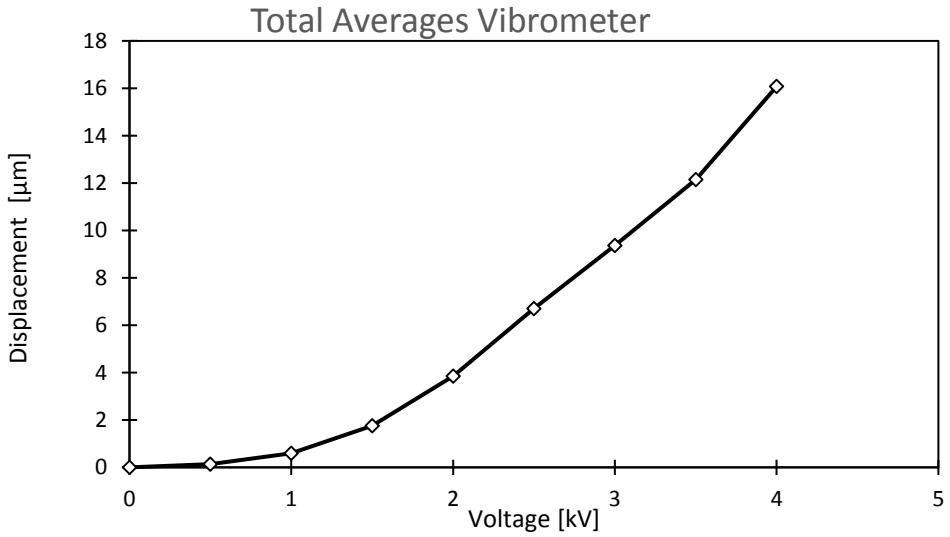

A.9. AC voltage superimposition experimental data

Sample 1

λ	C [pF]	C [pF]	C [pF]	d [µm]	d [µm]	d [µm]
4.40	1000 Hz	100 Hz	10 Hz	1000 Hz	100 Hz	10 Hz
	121.48	915.09	1698.34	0	0	0
	137.18	743.62	1387.40	1.533790244	-5.99539965	-5.82710779
	51.67	244.82	1429.78	-13.8669543	-71.1822887	-4.88367129
	16.75	178.20	1472.10	-44.0163558	-107.513514	-3.99573106
	8.40	29.12	846.55	-72.8877072	-790.92927	-26.1609392

Sample 2

λ	C(pF)	C(pF)	C(pF)	d [µm]	d [µm]	d [µm]
4.40	1000 Hz	100 Hz	10 Hz	1000 Hz	100 Hz	10 Hz
	11.12	828.82	1365.96	0	0	0
	21.08	803.71	1378.98	7.11456438	-0.40312482	0.123037903
	18.81	639.09	1394.69	6.008806971	-3.60890913	0.269204837
	4.48	444.51	893.01	-14.9686011	-9.50293415	-6.15616401
	0.43	53.53	438.02	-105.990629	-76.3104956	-19.9137837

Sample 3

λ	C(pF)	C(pF)	C(pF)	d [µm]	d [µm]	d [µm]
4.40	1000 Hz	100 Hz	10 Hz	1000 Hz	100 Hz	10 Hz
	264.78	1501.27	1326.12	0	0	0
	212.18	576.57	1346.31	-3.04468988	-15.9541529	0.195736786
	187.22	420.99	1388.61	-4.92043356	-23.0982842	0.591733629
	63.65	211.33	1244.21	-27.0281061	-43.2975537	-0.84219315
	1.71	163.05	323.51	-297.358417	-52.894245	-26.640637

Sample 4

λ	C(pF)	C(pF)	C(pF)	d [µm]	d [µm]	d [µm]
4.40	1000 Hz	100 Hz	10 Hz	1000 Hz	100 Hz	10 Hz
	385.31	919.85	1294.83	0	0	0
	636.54	970.33	1423.38	5.771283567	0.685332909	1.201905635
	589.39	740.16	1433.64	4.97770122	-2.98474783	1.29078798
	19.50	428.93	1207.39	-89.5695445	-12.0747667	-0.92496278
	1.21	556.41	479.18	-437.886414	-7.42976418	-16.7397369

Sample 5

λ	C(pF)	C(pF)	C(pF)	d [µm]	d [µm]	d [µm]
4.40	1000 Hz	100 Hz	10 Hz	1000 Hz	100 Hz	10 Hz
	18.81	220.71	1383.78	0	0	0
	148.72	345.19	1158.18	16.75344291	5.209919147	-2.41958908
	85.10	198.92	1093.71	13.77612304	-1.38739396	-3.24528948
	43.13	89.50	544.61	8.82877221	-14.829268	-15.4442737
	0.72	32.63	208.59	-106.625729	-41.6210785	-40.9665978

Bibliography

[1] J. Plante and S. Dubowsky, "Large scale failure modes of delectric elastomer actuators," *International Journal of Solids and Structures*, vol. 43, pp. 7727–7751, 2006.

[2] I. A. Anderson, T. A. Gisby, T. G. McKay, B. M. O'Brien, and E. P. Calius, "Multi-functional dielectric elastomer artificial muscles for soft and smart machines," *Journal of Applied Physics*, vol. 112, p. 041101, 2012.

[3] A. N. Norris, "Comment on method to analyze electromechanical stability of dielectric elastomers," 2013.

[4] F. Carpi, D. D. Rossi, R. Kornbluh, R. Pelrine, and P. Sommer-Larsen, *Dielectric Elastomers as Electromechanical Transducers*. Elsevier, 2007.

[5] A. R. Blythe, *Electrical properties of polymers*. Cambridge Universe Press, 1977.

[6] L. A. Toth and A. A. Goldenberg, "Control system design for a dielectric elastomer actuator: the sensory subsystem," *Proceedings of SPIE*, vol. 4695, pp. 323–334, 2002.

[7] S. H. Crandall, D. C. Karnopp, E. Kurtz, and D. C. Pridmore-Brown, *DDynamic of Mechanical and Electromechanical Systems*. Krieger Publishing Company, 1982.

[8] W. Lai, "Characteristics of dielectric elastomers and fabrication of dielectric elastomer actuators for artificial muscle applications," Master's thesis, Iowa State University, 2011.

[9] G. Kofod, "The static actuation of dielectric elastomer actuators: how does prestretch improve actuation?" *Journal of Physics D: Applied Physics*, vol. 41, p. 215405, 2008.

[10] D. J. Griffiths, *Introduction to Electromagnetics*, 3rd ed. Addison Wesley, 1999.

[11] A brief introduction to tensors and their properties. School of Engineering, Brown University. [Online]. Available: http://www.brown.edu/Departments/Engineering/Courses/En221/Notes/Tensors/Tensors.htm

[12] R. W. Ogden, G. Saccomandi, and I. Sgura, "Fitting hyperelastic models to experimental data," *Computational Mechanics*, vol. 34, pp. 484–502, 2004.

[13] M. Wissler and E. Mazza, "Mechanical behavior of an acrylic elastomer used in delectrid elastomer actuators," *Sensors and Actuators A: Physical*, vol. 134, pp. 494–504, 2007.

[14] N. C. Goulbourne, "A constitutive model of polyacrylate interpenetrating polymer networks for dielectric elastomers," *International Journal of Solids and Structures*, vol. 48, pp. 1085–1091, 2011.

[15] R. Díaz-Calleja, P. Llovera-Segovia, J. J. Dominguez, M. C. Rosique, and A. Q. Lopez, "Theoretical modelling and experimental results of electromechanical actuation of an elastomer," *Journal of Physics D: Applied Physics*, vol. 46, p. 235305, 2013.

[16] *Comsol Multiphysics User's Guide*, COMSOL, May 2012.

[17] R. Pelrine, R. Kornbluh, Q. Pei, S. Standford, S. Oh, and J. Eckerle, "Dielectric elastomer artificial muscle actuators toward biomimetic motion," *Proceedings of SPIE*, vol. 4695, pp. 126–137, 2002.

[18] S. J. A. Koh, C. Keplinger, T. Li, S. Bauer, and Z. Suo, "Dielectric elastomer generators: how much energy can be converted?" *Transactions on Mechatronics*, vol. 16, pp. 33–41, 2011.

[19] P. Prashanth, "Thermal evaporator," Center for Excellence in Nanoelectronics Indian Institute of Science, Tech. Rep.

[20] I. C. B. Association, "Carbon black user's guide safety, health, & environmental information," Online, June 2004.

[21] R. Pelrine, R. Kornbluh, J. Joseph, R. Heydt, Q. Pei, and S. Chiba, "High-field deformation of elelastomer dielectric for actuators," *Materials Science and Engineering C*, vol. 11, pp. 89–100, 1999.

[22] (2014, 5) Lesson 5: Expressing error in measurements. Online. studyphysics.ca.

[23] P. U. P. 152L, "Measurement analysis 1: Measurement uncertainty and propagation," Online.

[24] J. N. Reddy, *An Introduction to the Finite Element Method*, 3rd ed. McGraw-Hill, 2005.

[25] G. Kofod, P.Sommer-Larsen, R. Kornbluh, and R. Pelrine, "Actuation response of polyacrylate dielectric elastomers," *J. of Intell. Mater. Syst. and Struct.*, vol. 14, pp. 787–793, 2003.

[26] M. Wissler and E. Mazza, "Electromechanical coupling in dielectric elastomer actuators," *Sensors and Actuators A: Physical*, vol. 138, pp. 384–393, 2007, ogden parameters.

[27] A. F. Bower. (2009) Applied mechanics of solids. Online. [Online]. Available: http://solidmechanics.org/

[28] D. R. Clarke, J. Huang, S. Shian, R. M. Diebold, and Z. Suo, "The thickness and stretch dependence of the electrical breakdown strength of an acrylic dielectric elastomer," *Applied Physics Letters*, vol. 101, p. 235305, 2012.

[29] S. Rosset, M. Niklaus, P. Dubois, and H. Shea, "Mechanical characterization of a dielectric elastomer microactuator with ion-implanted electrodes," *Sensors and Actuators A: Physical*, vol. 144, pp. 185–193, 2008.

[30] S. Rosset and H. R. Shea, "Flexible and stretchable electrodes for dielectric elastomer actuators," *Applied Physics A*, 2012.

Nomenclature

α_i	Ogden constant
$\bar{P}$	Material frame coordinate
$\bar{p}$	Spatial frame coordinate
$\bar{u}$	Deformation vector
λ	Strain
λ_{act}	Actuated strain
λ_{pre}	Pre-stretched strain
μ_0	Vacuum permeability
μ_i	Ogden constant
∇	Nable operator
ρ	Total charge density
ε_0	Vacuum permittivity
ε_r	Relative permittivity
A	Area
B	Magnetic field
C	Capacity
c	Speed of light
D	Displacement field
$dnTz$	Maxwell downward normal stress tensor in the z direction
E	Electric field
E	Young's modulus

es	Comsol's electrostatics module
F	Deformation gradient
I	Identity tensor
J_f	Current density
K	Bulk modulus
L_i	Initial length
l_i	Actuated length
P	Electrostatic pressure on one side
P_{el}	Electrostatic pressure
p_{el}	Electrostatic pressure
Q	Charge
$T_{maxwell}$	Maxwell stress tensor
u	Deformation component in x direction
V	Voltage
v	Deformation component in y direction
W	Strain energy density
w	Deformation in z direction
DEA	Dielectric elastomer actuator
FEM	Finite element method

Auteursrechtelijke overeenkomst

Ik/wij verlenen het wereldwijde auteursrecht voor de ingediende eindverhandeling:
Electroactive properties of elastomers: finite element method modelling and experimental measurements

Richting: **master in de industriële wetenschappen: elektromechanica**
Jaar: **2014**

in alle mogelijke mediaformaten, - bestaande en in de toekomst te ontwikkelen - , aan de Universiteit Hasselt.

Niet tegenstaand deze toekenning van het auteursrecht aan de Universiteit Hasselt behoud ik als auteur het recht om de eindverhandeling, - in zijn geheel of gedeeltelijk -, vrij te reproduceren, (her)publiceren of distribueren zonder de toelating te moeten verkrijgen van de Universiteit Hasselt.

Ik bevestig dat de eindverhandeling mijn origineel werk is, en dat ik het recht heb om de rechten te verlenen die in deze overeenkomst worden beschreven. Ik verklaar tevens dat de eindverhandeling, naar mijn weten, het auteursrecht van anderen niet overtreedt.

Ik verklaar tevens dat ik voor het materiaal in de eindverhandeling dat beschermd wordt door het auteursrecht, de nodige toelatingen heb verkregen zodat ik deze ook aan de Universiteit Hasselt kan overdragen en dat dit duidelijk in de tekst en inhoud van de eindverhandeling werd genotificeerd.

Universiteit Hasselt zal mij als auteur(s) van de eindverhandeling identificeren en zal geen wijzigingen aanbrengen aan de eindverhandeling, uitgezonderd deze toegelaten door deze overeenkomst.

Voor akkoord,

Vorias, Raphaël **Letihon, Dimitri**

Datum: **27/08/2014**